© 2021. Published by The Company of Biologists Ltd | Journal of Cell Science (2021) 134, jcs258768. doi:10.1242/jcs.258768

RESEARCH ARTICLE

Differential gene regulation in DAPT-treated Hydra reveals candidate direct Notch signalling targets

Jasmin Moneer[1], Stefan Siebert[2], Stefan Krebs[3], Jack Cazet[2], Andrea Prexl[1], Qin Pan[1], Celina Juliano[2] and Angelika Böttger[1,*]

ABSTRACT

In *Hydra*, Notch inhibition causes defects in head patterning and prevents differentiation of proliferating nematocyte progenitor cells into mature nematocytes. To understand the molecular mechanisms by which the Notch pathway regulates these processes, we performed RNA-seq and identified genes that are differentially regulated in response to 48 h of treating the animals with the Notch inhibitor DAPT. To identify candidate direct regulators of Notch signalling, we profiled gene expression changes that occur during subsequent restoration of Notch activity and performed promoter analyses to identify RBPJ transcription factor-binding sites in the regulatory regions of Notch-responsive genes. Interrogating the available single-cell sequencing data set revealed the gene expression patterns of Notch-regulated *Hydra* genes. Through these analyses, a comprehensive picture of the molecular pathways regulated by Notch signalling in head patterning and in interstitial cell differentiation in *Hydra* emerged. As prime candidates for direct Notch target genes, in addition to *Hydra* (*Hy*)*Hes*, we suggest *Sp5* and *HyAlx*. They rapidly recovered their expression levels after DAPT removal and possess Notch-responsive RBPJ transcription factor-binding sites in their regulatory regions.

KEY WORDS: Hydra, Notch pathway, Wnt pathway, Axis formation, Nematocyte differentiation

INTRODUCTION

Notch signalling facilitates cell fate decisions and pattern formation by inducing terminal differentiation and mediating lateral inhibition, boundary formation and synchronization of developmental processes in animals. Well-studied examples of Notch-regulated processes include the differentiation of the wing margin and the specification of neurons from neuroectoderm in *Drosophila* embryos and somite formation during vertebrate development (Liao and Oates, 2017; Siebel and Lendahl, 2017). The core components of the Notch pathway include the Notch receptor, the Delta/Serrate/Lag-2 (DSL) ligands and recombining binding protein suppressor of hairless (RBPJ) transcription factors [also called CSL, for CBF1 in mammals, Su(H) in *Drosophila* and Lag-1 in *Caenorhabditis*] (Andersson et al., 2011). Both the DSL ligands and Notch receptors are transmembrane proteins, therefore signalling occurs between directly adjacent cells. Interactions between DSL ligands and Notch receptors result in cleavage of the Notch receptor by presenilin followed by nuclear translocation of the intracellular domain of Notch (NICD) (reviewed in Mumm and Kopan, 2000). NICD works as a transcriptional co-activator of CSL factors.

Direct target genes of Notch signalling have been identified previously (reviewed by Giaimo et al., 2021; Wang et al., 2015). Targets of Notch signalling are activated or repressed in different cell types depending on the composition of transcriptional complexes induced by Notch activity and the epigenetic status at the respective loci. A primary and evolutionarily conserved target of Notch is the Hey-Hes family of transcriptional repressors. Other context-dependent direct target genes of Notch signalling that have been identified include *Myc*, cyclin D1 and *MEK5c* in tumour cells (reviewed in Borggrefe and Oswald, 2009). In hematopoietic cells, *GATA3*, the master regulator for T-cell development, and several Hox genes are direct Notch targets (Fang et al., 2007). Genome-wide analysis in *Drosophila* has shown that genes of the epidermal growth factor receptor pathway are direct targets of Notch signalling and it showed that Notch targeted activators and repressors of certain genes at the same time (Krejci et al., 2009). Notch also induces transcription of its own inhibitors, for example, the small Notch-regulated ankyrin repeat protein NRARP (Jarrett et al., 2019).

To reveal the ancestral core regulatory network directed by the highly conserved Notch signalling pathway, we have focused on a cnidarian, the fresh water polyp *Hydra*. As a sister to bilaterian animals, cnidarians hold an informative phylogenetic position. Moreover, *Hydra* provides the unique opportunity to obtain an animal-wide picture of Notch target genes with cell-type resolution due to the recently available single-cell expression map (Siebert et al., 2019).

Hydra polyps have a simple body structure, representing a tube with an oral head structure and an aboral foot. The head consists of the hypostome, with a central mouth opening surrounded by a crest of tentacles. The foot consists of a peduncle, terminating in the basal disc. The body column of the polyp is composed of two epithelial monolayers, termed ectoderm and endoderm, separated by an acellular extracellular matrix, the mesoglea. Ectoderm and endoderm are self-renewing epithelial cell lineages. A third cell lineage, the interstitial cells, resides in interstitial spaces of both epithelia (David and Campbell, 1972; David and Gierer, 1974). It is supported by self-renewing multipotent stem cells, which provide a steady supply of neurons, gland cells and nematocytes. Nematocytes are cnidarian-specific sensory cells, which harbour the nematocyst or cnidocyst used for capturing prey. Epithelial cells divide along the entire body column of the polyps

[1]Ludwig Maximilians-University Munich, Germany, Biocenter, 82152 Planegg-Martinsried, Großhaderner Str. 2, Germany. [2]Department of Molecular and Cellular Biology, University of California, Davis, CA 95616, USA. [3]Ludwig-Maximilians-University Munich, Gene Center Munich, Feodor-Lynen-Str. 25 81377 Munich, Germany.

*Author for correspondence (boettger@zi.biologie.uni-muenchen.de)

J.C., 0000-0002-7331-5631; A.P., 0000-0001-8951-4654; A.B., 0000-0003-3273-9558

Handling Editor: John Heath
Received 8 April 2021; Accepted 3 May 2021

Journal of Cell Science (2021) 134, jcs258768. doi:10.1242/jcs.258768

(Holstein et al., 1991) leading to the displacement of cells towards the oral and aboral ends, and into asexually produced buds. Cells arriving at the base of tentacles or at the basal disc cease cell division and induce differentiation into tentacle or basal disc cells. Buds develop into new polyps and are then released from the parent polyp. Sexual reproduction occurs when interstitial lineage derived germ cells develop into egg and sperm cells (Bosch and David, 1986). Ectodermal tentacle cells are battery cells, where each cell harbours several mature nematocytes. Older cells are shed at the tips of the tentacles and the foot. Owing to continual cell divisions, almost all *Hydra* cells are replaced approximately every 20 days (Otto and Campbell, 1977). Therefore, the homeostatic animal is in a constant state of development requiring the presence of signalling for patterning the body axis and direct cell fate specification (Steele, 2002).

The *Hydra* Notch pathway components include the receptor HvNotch (Hv for *Hydra vulgaris*), the ligand HyJagged (Hy for *Hydra*) and the CSL-homolog, HvSu(H). The basic mechanisms of Notch signalling are conserved in *Hydra*, including regulated intramembrane proteolysis (RIP) through presenilin, followed by nuclear translocation of the NICD (reviewed in Mumm and Kopan, 2000). Moreover, the promoter of the *Hydra* HES-family member *HyHes* can be activated by the HvNotch NICD indicating that *HyHes* is a direct target of Notch signalling (Käsbauer et al., 2007; Münder et al., 2010; Prexl et al., 2011).

The presenilin inhibitor DAPT efficiently blocks nuclear translocation of NICD and phenocopies Notch loss-of-function mutations in *Drosophila* and zebrafish (Geling et al., 2002; Micchelli et al., 2003). In the cnidarians *Nematostella vectensis* and *Hydractinia echinata*, morpholino-mediated knockdown or CRISPR-Cas-mediated mutagenesis of Notch results in comparable phenotypes to those seen upon DAPT treatment in both organisms, with them displaying defects in nematocyte differentiation and tentacle patterning (Gahan et al., 2017; Marlow et al., 2012; Richards and Rentzsch, 2015).

In *Hydra*, we have shown that DAPT treatment inhibits NICD translocation, which results in four strong effects. First, DAPT blocks post-mitotic differentiation in the nematoblast and germ cell lineages. Early differentiating nematocytes are genetically specified by the expression of the achaete-scute homolog *CnASH* (*Cn* for Cnidarian) (Grens et al., 1995; Lindgens et al., 2004) and morphologically by the presence of a post-Golgi vacuole as an element of capsule development. This cell state disappears in DAPT treated animals. Second, DAPT blocks post-mitotic differentiation of female germ cells causing proliferating germ cell precursors to form tumour-like growths (Alexandrova et al., 2005; Käsbauer et al., 2007). Third, DAPT impairs boundary formation at both parent–bud and body column–tentacle boundaries in such a way that the typically sharp gene expression border margins at these structures become diffuse. At the parent–bud boundary this misexpression of the *Hydra* FGF-R-homolog *kringelche*n leads to failure of bud foot formation and detachment (Münder et al., 2010; Sudhop et al., 2004). At the base of tentacles, *HyAlx* expression, which demarcates the tentacle boundaries (Smith et al., 2000), becomes diffuse and we observe malformations of the head structure (Münder et al., 2013). Fourth, DAPT inhibits *Hydra* head regeneration and regenerating tissue is not able to re-establish an oral organiser as evidenced by lack of Wnt-3 expression. This leads to failure in developing a properly patterned head with hypostome and evenly spaced tentacles (Münder et al., 2013).

To gain a better understanding of the underlying molecular causes of the Notch inhibition phenotypes, we aimed to identify the transcriptional target genes of Notch signalling. We identified 831 genes that were differentially expressed in response to 48 h of DAPT treatment; 75% of these were downregulated. Single-cell expression data were used to uncover the gene expression patterns at cell-state resolution for the Notch-responsive genes. We found that Notch-responsive genes were expressed in cell states such as differentiating nematocytes and oral cell types, which is consistent with the DAPT-induced phenotypes. To identify potential direct targets of Notch signalling, we also profiled the gene expression changes that occurred immediately after DAPT removal. Investigating the expression dynamics of Notch responsive genes and performing motif enrichment analysis enabled us to predict likely direct targets of Notch signalling in *Hydra*.

RESULTS

Differential gene expression analysis reveals Notch-responsive genes

To identify targets of Notch signalling in *Hydra*, we elucidated transcriptional changes that occur in response to DAPT treatment. We expected that sustained DAPT treatment would result in the misregulation of both direct and indirect Notch targets. We furthermore predicted that direct targets would return to control expression levels after DAPT removal more quickly than indirect targets. We profiled gene expression changes immediately after 48 h of sustained DAPT treatment (0 h time point) to identify all Notch-affected genes. In addition, we profiled gene expression 3 and 6 h after DAPT removal to monitor the recovery of these Notch-affected genes.

To characterise the 3 and 6 h time points after DAPT removal we used reverse transcription quantitative real-time PCR (RT-qPCR) to monitor the expression levels of two genes: (1) *HyHES*, which is a known direct Notch target (Münder et al., 2010), and (2) *CnASH*, which is expressed in post-mitotic differentiating nematoblasts (Lindgens et al., 2004), a cell state that is lost in response to DAPT treatment (Käsbauer et al., 2007). Loss of *CnASH* expression is a secondary (or indirect) effect of Notch inhibition and re-establishment of *CnASH* expression will only occur after DAPT removal once nematogenesis is restored.

As expected, both *HyHES* and *CnASH* were downregulated after 48 h of DAPT treatment. *HyHES* expression returned to normal levels between 5.5 and 8 h after inhibitor removal, whereas *CnASH* expression was still downregulated after 24 h (Fig. S1). RNA-seq was therefore performed on tissue samples collected after 48 h DAPT treatment (0 h) and at the 3 h and 6 h time points after DAPT removal, since the 6 h intervals appeared sufficient to distinguish direct from indirect Notch-targets and the 3 h intervals were added to monitor earliest responses in gene expression after resuming NICD activity. The workflow for this experiment is illustrated in Fig. 1.

Genes that were differentially expressed after 48 h of DAPT treatment (time point 0 h) were referred to as Notch-responsive genes (NR genes). Of the 831 NR genes identified, 624 were downregulated (75%) and 207 were upregulated (25%) (Fig. 2A). Clustering NR genes according to their fold changes (Fig. 2B) at the three time points after DAPT removal (0 h, 3 h, and 6 h) revealed 279 genes (201 down, 78 up) genes with re-established expression levels at 3 h, including the confirmed Notch target *HyHES*. A total of 194 genes (143 down, 51 up) showed re-established expression by 6 h and 313 genes (243 down, 70 up) were still differentially expressed at 6 h, including *CnASH*. A total of 45 genes, including *CnGSC*, were differentially expressed at time points 0 h and 6 h, but not at 3 h (Fig. 2A, 'Other'). In addition, 160 genes were found to be

Journal of Cell Science (2021) 134, jcs258768. doi:10.1242/jcs.258768

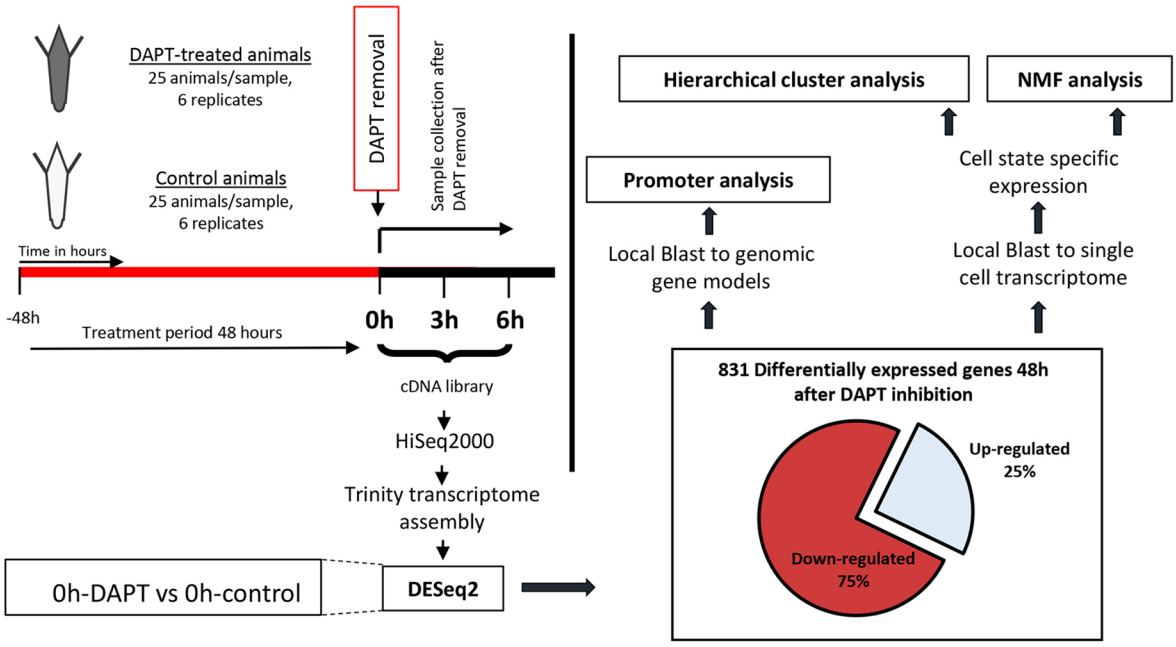

Fig. 1. Overview of the experimental and analysis workflow. *Hydra* polyps were treated with either DAPT or DMSO (control) for 48 h. Thereafter, total RNA for sequencing was collected at three time points. The sample 0 h was taken immediately after 48 h of DAPT treatment. This is also the time point at which DAPT was removed from the samples and total RNA was collected 3 and 6 h after DAPT removal. Six biological replicates for each treatment were collected and processed at the same time point. Pairwise differential gene expression analysis by DESeq2 was performed between DAPT- and DMSO-treated samples for each of the three collection time points. This analysis revealed 831 Notch-responsive genes (NR genes) after 48 h of DAPT treatment (0 h). For these genes we characterized the expression at time points 3 h and 6 h. For 666 NR genes single-cell expression data from homeostatic polyps were available (Siebert et al., 2019) and was used to elucidate expression pattern and cell-state-specific expression using hierarchical cluster and non-negative matrix factorization (NMF) analysis. Additionally, motif enrichment was performed for the set of NR genes.

differentially expressed at 3 and/or 6 h, but not at 0 h. These were excluded from further analysis.

Overall, these data reveal changes in gene expression caused by inhibition of the Notch pathway, and uncover which changes are rapidly reversed upon relief of this inhibition. This allowed us to explore the cell type-specific effects of DAPT treatment and identify possible direct targets of Notch signalling [the full list of NR genes is available via Figshare (doi:10.6084/m9.figshare.14681343)].

Single-cell expression data demonstrate nematogenesis and epithelial expression of Notch-responsive genes

Next, we elucidated NR gene expression patterns by exploring *Hydra* single-cell expression data, which were available for 666 (80%) NR genes (Fig. 1). We defined cell state and spatial expression of NR genes on the basis of published cell state annotations (Siebert et al., 2019). Hierarchical cluster analysis revealed groups of genes expressed in specific cell states (Fig. 3): nematoblasts/nematocytes (violet, red, blue and yellow clusters, 315 genes), ectodermal epithelial cells, including battery cells (black cluster, 90 genes), endodermal epithelial cells including tentacle cells (grey cluster, 80 genes), and genes more ubiquitously expressed across cell states (cyan cluster, 79 genes). An additional small subset comprising 102 NR genes included genes with restricted expression in several distinct cell states, such as specific neurons, gland cells, germline cells or ectodermal basal disc cells (green cluster, 102 genes). The majority of these 666 NR genes fell into two broad categories: (1) 47% that were specifically expressed in nematoblasts and nematocysts, and (2) 25% that were specifically expressed in epithelial cells (black and grey cluster, Fig. 3).

In addition, we performed non-negative matrix factorisation (NMF) on the NR gene set as an unbiased means to uncover modules of co-expressed genes (metagenes) and identified 23 metagenes. We then visualized metagene expression on the t-distributed stochastic neighbour embedding (tSNE) representation of selected clusterings from Siebert et al. (2019) (Fig. S2). The NMF analysis identified cell-state-specific modules that were consistent with the hierarchical clustering results (Fig. S2; Fig. 3). Interestingly, a single metagene was found to be expressed in female germ line cells, suggesting Notch function during female gametogenesis (Fig. S2G).

Nematoblast and nematocyte expression of NR genes

The largest fraction of NR genes have nematoblast- or nematocyte-specific expression. In *Hydra*, this lineage comprises four types of nematocytes, each of which harbours a single capsule (or nematocyst) of the atrichous isorhiza, holotrichous isorhiza, stenotele or desmoneme type. Nematocytes develop from interstitial stem cells via a proliferative amplification phase with incomplete cytokinesis that results in the formation of nests of 4, 8, 16, and 32 nematoblasts. The cells in these nests undergo a final mitosis and start capsule morphogenesis, a process that can be divided into five stages: (1) formation of a growing capsule primordium from a large post-Golgi vacuole, (2) growing of a tubule elongation of the capsule, (3) invagination of the tubule into the capsule, (4) formation of spines inside the invaginated tubule and (5) hardening of the capsule wall. Nests with mature nematocytes break up, and single nematocytes then get incorporated into the battery cells of the tentacles or into epithelial cells of the body column (David and Gierer, 1974; Engel et al., 2002).

As Notch inhibition by DAPT treatment results in a severe block of nematocyte differentiation, which occurs coincident with or immediately after mitotic exit of differentiating nematoblasts

Journal of Cell Science (2021) 134, jcs258768. doi:10.1242/jcs.258768

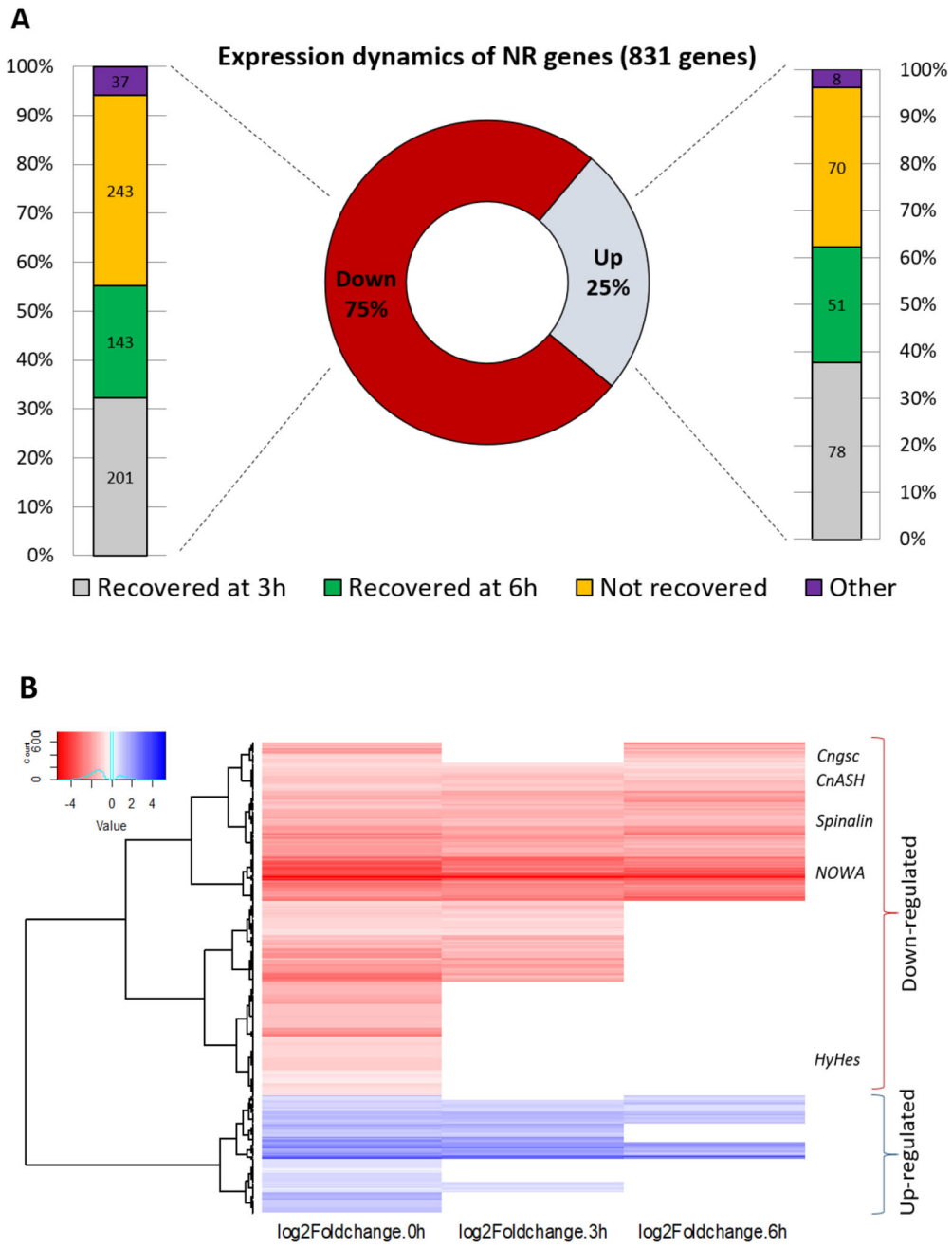

Fig. 2. Differential expression of NR genes post DAPT treatment. (A) Expression dynamics of differentially expressed NR genes and time points for the recovery of original expression levels. For both up- and down-regulated genes, ∼35% recover original expression within the first 3 h (‘Recovered at 3h’, grey), ∼25% recover within 6 h (‘Recovered at 6h’, green), and ∼30–40% do not recover original expression within the time course of the experiment (‘Not recovered’, yellow). The remaining genes (∼5%, ‘Other’, purple) behave irregularly, e.g. recovered after 3 h, deregulated again after 6 h. (B) Heatmap highlighting expression differences of all 831 NR genes. The colour key refers to the $\log_2$ fold change values. The cyan line in the small diagram indicates the distribution of *z*-scores. Clustering of NR genes by their log2Foldchange for each time point revealed upregulated (blue) and downregulated (red) genes. No value (white background) means the gene was not differentially expressed at that particular time point and thus had control expression levels. We identified sets of genes that recover their expression by 3 h (e.g. *HyHes*, differentially expressed at 0 h, thereafter back to control expression level), genes that recover expression by 6 h, and genes that do not recover expression during the course of the experiment, i.e. at 6 h after DAPT removal (e.g. the post-mitotic nematocyte gene markers *CnASH*, *NOWA* and *Spinalin*). A fourth set includes genes that are differentially expressed at 0 h and 6 h, but not at the 3 h time point (e.g. *CnGSC*).

(Käsbauer et al., 2007), we sought to identify the exact differentiation step that was affected. We therefore performed hierarchical clustering for NR genes with expression in nematoblast or nematocyte cell states (Fig. 3, violet, red, blue and yellow clusters) using the *Hydra* single-cell data (Siebert et al., 2019). The single-cell data revealed four distinct nematocyte differentiation trajectories, and gene expression state changes were identified along these trajectories from stem cells to differentiated nematocytes. Moreover, the single-cell analysis revealed eight distinct nematoblast stages along these four trajectories (nb1 through nb8). Two of these trajectories are annotated as desmoneme and stenotele differentiation, based on marker gene expression (Siebert et al., 2019). In the present study, the clustering of NR genes expressed during nematogenesis revealed that the majority of those genes are strongly expressed in cell states nb4, nb5, nb6, nb7, nb8 and in differentiated nematocytes (nem), with no or much lower expression in the earlier cell states of interstitial stem cells (ISC.nb), nb1, nb2 and nb3 (Fig. 4A). This was also observed by plotting the expression of the NR gene modules onto the single-cell tSNE representation (Fig. S2) which indicates expression in all three nematocyte types including desmonemes (Fig. S2B), stenoteles (Fig. S2C) and isorhizas (Fig. S2D).

To identify the point in the trajectories in which differentiating nematoblasts transition from proliferating to post-mitotic nematoblasts, we looked at the expression profiles of two genes that mark proliferating nematoblasts: (1) proliferating cell nuclear antigen *PCNA* (t10355aep) and (2) the Zn-finger transcription factor gene zic/odd-paired homolog *Hydra-zic* (*Hyzic*) (t13359aep; Lindgens et al., 2004). *PCNA* expression is seen in states ISC.nb, nb1 and nb2 classifying them as proliferating nematoblasts (Fig. 5A). Nb1 and nb2 express HyZic, confirming that HyZic expression is restricted to proliferative nematoblast states as had

Journal of Cell Science (2021) 134, jcs258768. doi:10.1242/jcs.258768

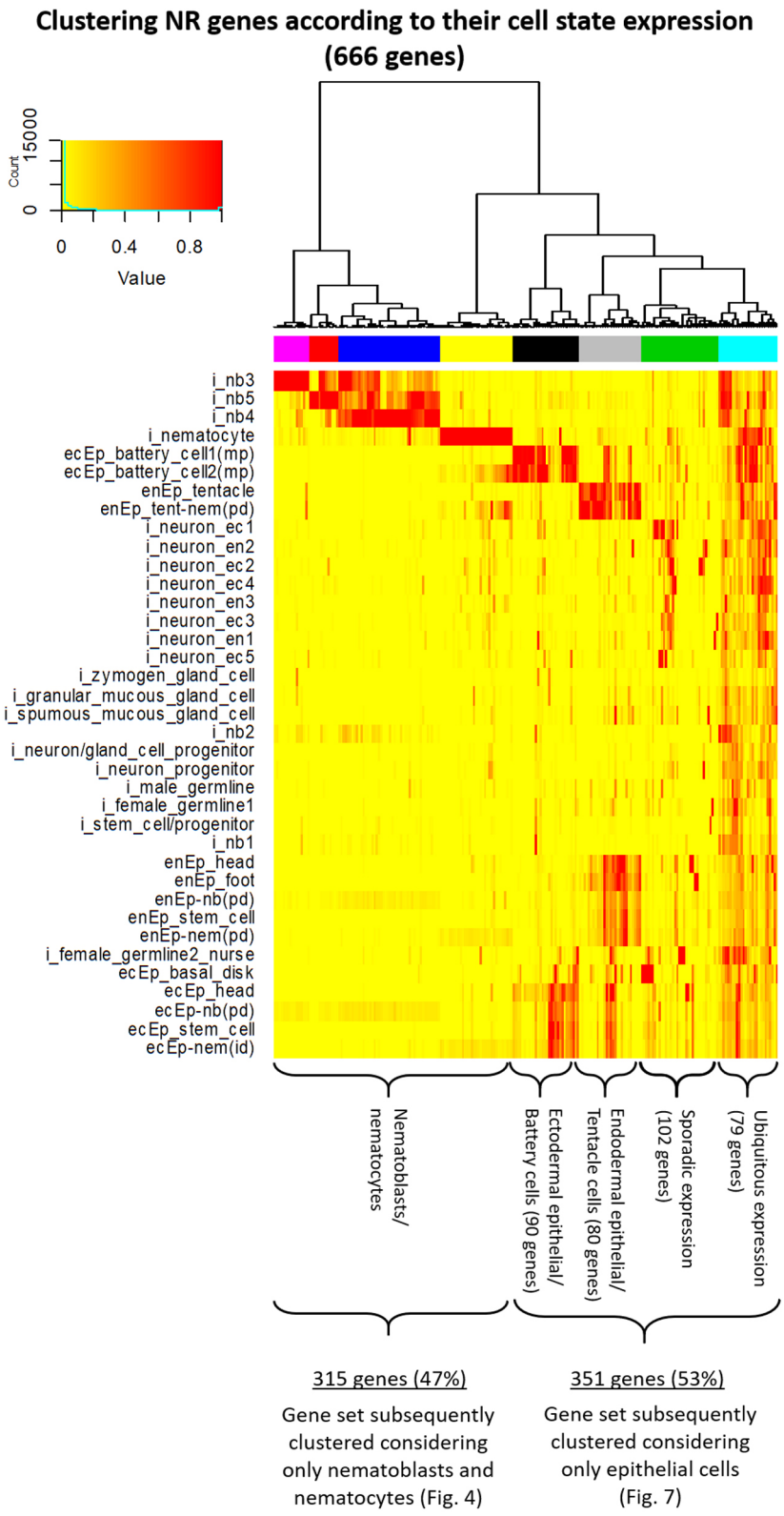

Fig. 3. NR gene expression in homeostatic polyps based on single-cell expression data. Expression data and cell state annotations were retrieved from Siebert et al. (2019). Hierarchical clustering was performed for 666 NR genes using average expression values for each annotated cell state. The colour key refers to cell state expression values. The green line in the small diagram indicates the distribution of *z*-scores. This revealed expression in nematoblast/nematocyte-specific genes (violet, red, blue and yellow cluster), ectodermal epithelial cell genes including battery cell genes (black), endodermal epithelial cell genes including tentacle genes (grey), genes ubiquitously expressed across a wide range of cell states (cyan) and genes with a sporadic expression (green). Nematoblast/nematocyte genes constituted 47% of the NR genes. i, cell of the interstitial lineage; nb, nematoblast; ecEp, ectodermal epithelial cell; enEP, endodermal epithelial cell; en, endoderm; ec, ectoderm.

been shown before (Lindgens et al., 2004). The absence of PCNA-expression in cell states nb3 and nb4 suggests that these are the earliest post-mitotic nematoblasts producing the nematocyst spine and inner wall protein spinalin (Käsbauer et al., 2007; Koch et al., 1998) and *spinalin* expression is clearly seen in these cells (Fig. 5A). Expression of the early differentiation marker genes *NOWA* and *CnASH* become detectable in differentiation states nb5 through nb8 when nematocyst capsules are formed (Fig. 5A,C).

As further evidence that *HyZic* and *CnASH* mark mitotic and post-mitotic stages of nematogenesis respectively, using immunofluorescence we show that CnASH protein is detected in the cytoplasm of nematoblasts that contain vacuoles, which were

Journal of Cell Science (2021) 134, jcs258768. doi:10.1242/jcs.258768

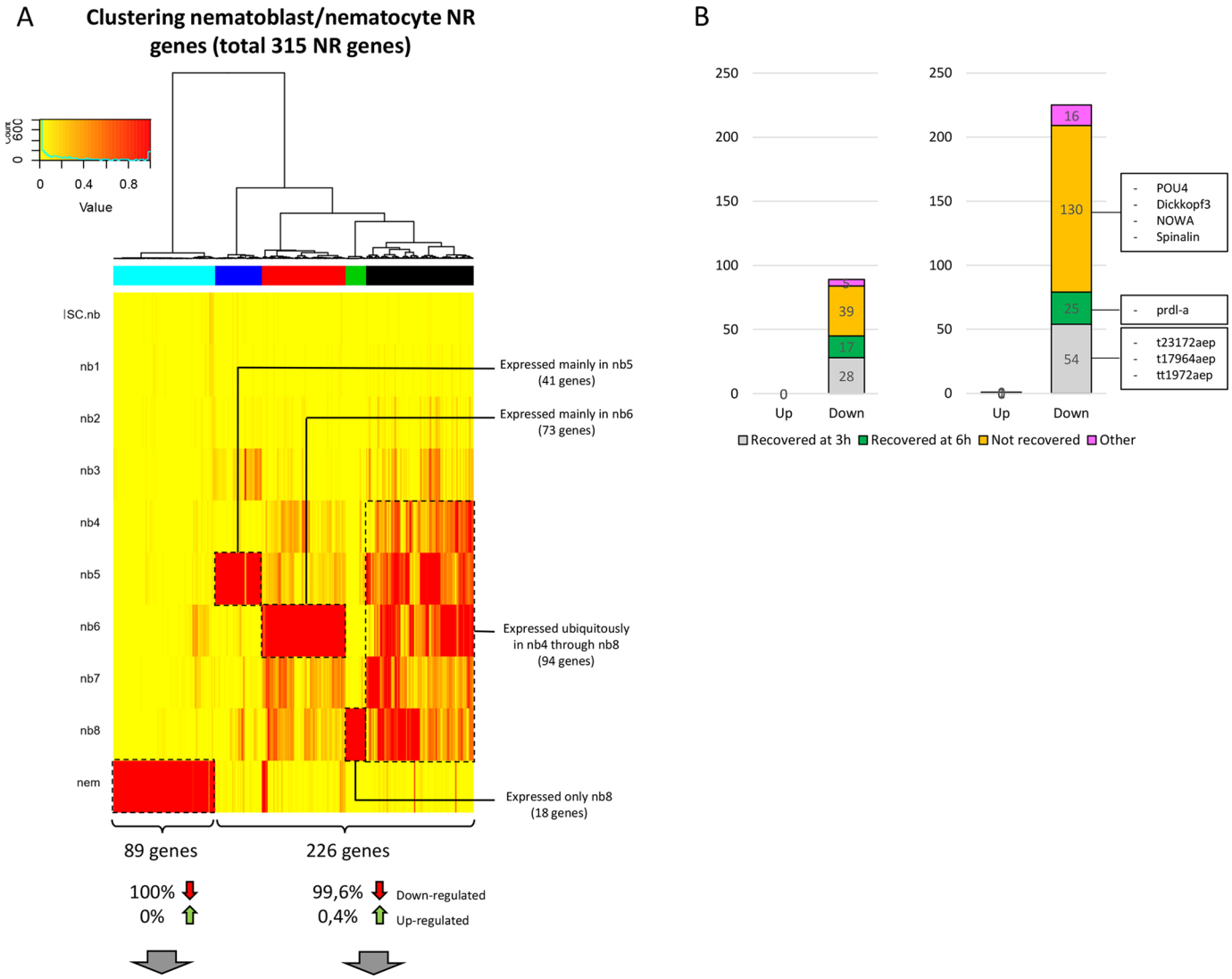

Fig. 4. Hierarchical clustering of NR genes expressed in the nematocyte lineage. (A) NR genes expressed in cells of the nematocyte lineage were clustered separately to reveal their expression in the differentiation states of nematogenesis. This revealed a set of genes only expressed in mature nematocytes (cyan cluster), genes mainly expressed in cell state nb5 (blue), genes mainly expressed in nb6 (red), genes mainly expressed in nb8 (green) and genes expressed ubiquitously in stages nb4 through nb8 (black). Almost all of these genes were downregulated upon DAPT treatment. (B) The majority of both mature nematocyte genes and nematoblast genes did not recover their expression 6 h after DAPT removal (yellow). This includes POU4, Dickkopf3, NOWA and Spinalin. Furthermore, genes are represented that recovered after 3 h (grey), 6 h (green) or that had an irregular recovery profile (magenta).

visualised with anti-NOWA antibody (Engel et al., 2002). By contrast, HyZic protein was detected in the cytoplasm of nematoblasts without visible vacuoles and not found in CnASH positive nematoblasts (Fig. 5B).

Of the 315 NR genes that are expressed in nematoblasts or nematocytes, 314 were downregulated upon Notch-inhibition (Fig. 4A). These downregulated genes include many genes expressed in developing nematocytes such as *POU4* (t11335aep), *Prdl-a* (t21636aep; Gauchat et al., 2004), *HyDickkopf 3* (t20111aep; similar to *HyDKK3*; Fedders et al., 2004), *CnASH* (t10853aep, Grens et al., 1995; Figs 4B and 5B), *NOWA* (t15237aep; Engel et al., 2002) and *Spinalin* (t38568aep; Koch et al., 1998), this gene has now three NCBI entries and encodes a longer protein than initially described [an alignment is available via FigShare (doi:10.6084/m9.figshare.14714169); Fig. 4B]. Using double *in situ* hybridization to detect *POU4* and *HyZic* transcripts, we found mutually exclusive expression of these two genes in differentiating nematocytes, which demonstrates that *POU4* is expressed in post-mitotic nematocytes (Fig. S3A). Using *in situ* hybridization, we also showed that HyZic-positive nematocytes were not affected by DAPT treatment, whereas *CnASH* and *POU4* expression was lost (Fig. S3B,C). As DAPT treatment causes the disappearance of post-mitotic differentiating nematocytes, which are recognised by their forming of post-Golgi vacuoles (Käsbauer et al., 2007), the seeming loss of *POU* and *CnAsh* expression after DAPT treatment (Fig. S3B, C) is caused by a loss of the developing nematocyte cell states expressing these genes.

More than 50% of the nematoblast-specific NR genes remained downregulated and did not recover their normal expression level within 6 h after the Notch-inhibitor was removed (Fig. 4B). This again suggests that downregulation of nematogenesis genes reflects the loss of cell states and is mainly an indirect effect of the block in this process caused by Notch inhibition. By contrast, some nematocyte-specific putative transcription factors did recover their expression levels quickly after DAPT removal. These included a possible class I member of the HMG box superfamily, similar to

Journal of Cell Science (2021) 134, jcs258768. doi:10.1242/jcs.258768

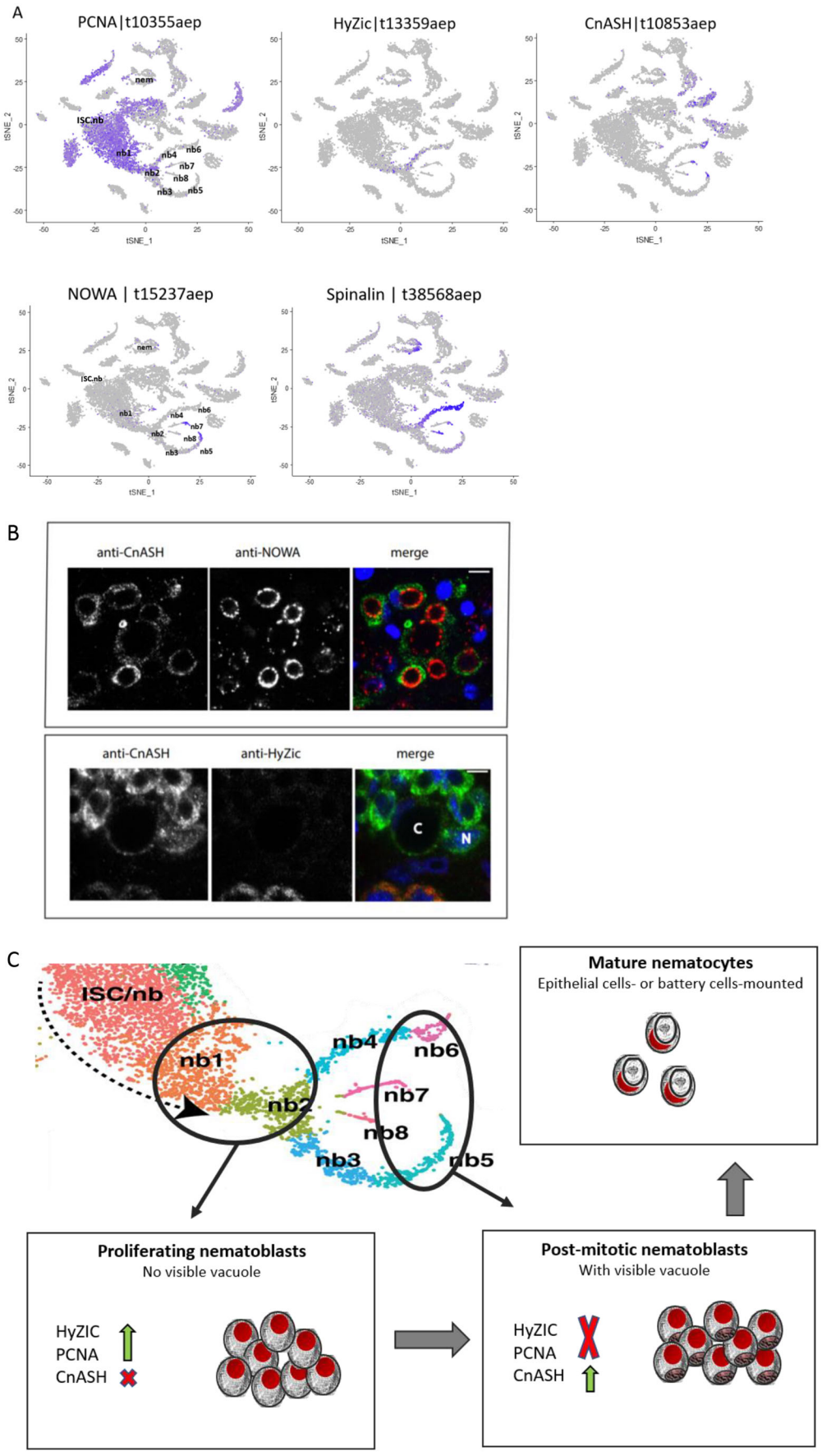

Fig. 5. Homeostatic expression of nematoblast marker genes and proteins. (A) t-Distributed stochastic neighbour embedding (t-SNE) representation showing the interstitial cell state expression of *HyZic*, *PCNA*, *CnASH*, *NOWA* and *spinalin*. Cluster labels are provided for cell states of the nematoblast lineage according to Siebert et al. (2019). nb, nematoblast; nem, nematocyte; ISC, interstitial stem cell. Blue dots indicate cells expressing the respective genes. *PCNA* is expressed in proliferating cells, nematoblast cell states nb1 and nb2. *HyZIC* is mainly expressed in nb2. This is in accordance with previously published work indicating *HyZIC* expression in proliferating nematoblasts. *CnASH* is expressed in nb5, 6, 7, 8, representing post-mitotic nematoblasts lacking PCNA expression. This is in complete agreement with previous work (Lindgens et al., 2004). *NOWA* encoding an outer capsule protein, is expressed in nb5 and nb7, *spinalin*, encoding a protein occurring inside the capsule, is expressed in nb4, 5, 6, 7 and 8 and in mature nematocytes (nem), all representing post-mitotic nematoblast stages. (B) Laser confocal microscopic sections of co-immunofluorescence staining with anti-HyZIC, anti-CnASH and anti-NOWA antibodies, in merged images DNA stain DAPI (blue), CnASH (green), HyZIC (red), NOWA (red). Anti-NOWA antibody delineates capsules (upper panel, middle image and red in merged). Co-staining with anti-CnASH antibody indicates signal in cytoplasm of capsule containing cells (upper panel, left hand image and green in merged). Capsule containing CnASH-positive cells (lower panel, left hand side and merged image green) are not stained with anti-HyZIC antibody (lower panel, middle image and merged image red); C, capsule; N, nucleus. Scale bars: 20 µm. (C) Schematic summary of gene expression in the nematoblast lineage indicating a differentiation pathway from interstitial stem cell precursors (ISC/nb) via proliferating PCNA and HyZIC expressing amplifying nematoblast precursors (nb1, nb2) via post-mitotic nematoblasts not expressing PCNA (nb3, nb4) to capsule forming CnASH expressing nematoblasts (nb5, 6, 7, 8), t-SNE representation of cells with clusters labeled by cell state as presented in Siebert et al. (2019) with permission. Images are representative of three experiments.

SOXB3 from *Hydractinia echinata* [t23172aep, XP_012555836.1; an alignment is available via FigShare (doi:10.6084/m9.figshare.14714169)], a protein with a C-terminal bZIP-Jun-domain [t17964aep; an alignment is available via FigShare (doi:10.6084/m9.figshare.14714169)] and a predicted forkhead box protein I1c-like [t1972aep, an alignment is available via FigShare (doi:10.6084/m9.figshare.14714169)], and (Fig. 4B). Given the rapid recovery of their expression after DAPT removal, these genes may be directly targeted by Notch signalling and possibly play a major role in driving nematogenesis.

In conclusion, our differential gene expression analysis confirms that inhibition of Notch signalling causes a decrease in gene expression in differentiating nematoblast stages, coinciding with the loss of this cell type within 48 h of DAPT treatment (Käsbauer et al., 2007). The gene expression of proliferating nematoblasts remained undisturbed.

Epithelial expression of Notch-regulated genes

About 25% of NR genes for which expression patterns were available had enriched expression in epithelial cells (Fig. 3, black and grey cluster) while the remaining non-nematoblast NR genes showed either sporadic or ubiquitous expression (Fig. 3, cyan and green clusters).

Since previous Notch inhibition studies demonstrated severe malformations of the *Hydra* head structure (Münder et al., 2013), we aimed to elucidate the effect of DAPT treatment on epithelial body column cells and their derivatives (e.g. specialized head and foot cells). Hierarchical clustering using single-cell data for epithelial cells revealed genes that were expressed (1) in all endodermal and ectodermal epithelial cell types along the oral-aboral axis (Fig. 6, grey cluster), (2) mainly in ectodermal epithelial cells (Fig. 6, cyan cluster) and (3) mainly in endodermal epithelial cells (Fig. 6, green cluster). The majority of these epithelial genes from the grey, cyan and green clusters were upregulated in response to DAPT treatment (Fig. 6). These included 36 genes associated with ER, Golgi and endosomal proteins, such as proteins involved in glycosylation like the oligosaccharyl transferase DAD1(t14233aep|DAD1), a negative regulator of cell death (Roboti and High, 2012). Some were involved in redox regulation and unfolded protein response and some were chaperones [see tables on FigShare; full list of NR genes (doi:10.6084/m9.figshare.14681343) and functional annotation of NR genes: (doi:10.6084/m9.figshare.14681319)]. Moreover, membrane proteins, including 12 G-protein coupled receptors, caspase D (t7281aep; Lasi et al., 2010) and the homolog of the ubiquitin-ligase and Notch-modulator mind bomb were also upregulated (t3105aep). Thus, many of the upregulated epithelial genes seem to be involved in stress responses to DAPT treatment. In contrast, *Sp5*, which is involved in *Hydra* head patterning (t29291aep; Vogg et al., 2019) was downregulated (Fig. 7A).

Two sets of genes comprised tentacle genes expressed in endodermal tentacle cells (Fig. 6, red cluster) and in ectodermal battery cells (Fig. 6, black cluster). In both sets, the majority of genes were downregulated upon Notch inhibition (88% of battery cell genes and 71% of endodermal tentacle genes). These included a gene encoding a Na^+ channel in battery cells (t18364aep; Golubovic et al., 2007) and the collagen gene Hcol1 (t14477; Deutzmann et al., 2000) in endodermal tentacle cells (Fig. 7B). The endodermal matrix metalloprotease gene HMMP was upregulated (t16424aep; Leontovich et al., 2000). Both extracellular matrix genes, HMMP and Hcol1, recovered their expression levels within 3 h (Fig. 7B).

Furthermore, small sets of NR genes were specifically expressed in (1) ectodermal head cells, (2) endodermal head cells, and (3) endodermal foot cells (Fig. 6, included in cyan and green clusters). Another NR gene cluster was expressed in ectodermal basal disc cells (Fig. 6, yellow cluster). These expression patterns also could be seen on tSNE plots after NMF analysis (see Fig. S2I,L,M).

The NR genes expressed in endodermal and ectodermal head cells were largely downregulated and several of these have known functions in head patterning. Of note, *HyALX* (t16456aep; Smith et al., 2000) is expressed at tentacle boundaries and previous work demonstrated that HvNotch is needed to maintain this expression pattern (Münder et al., 2013). Furthermore, several potential head organizer genes including *Wnt7* (t28874aep; Lengfeld et al., 2009), the transcription factor gene *TCF* (t11826aep; Hobmayer et al., 2000), an Otx-related homeodomain protein (t33622aep), an FGF homolog (t8338aep; annotation confirmed by Monika Hassel, Marburg, Germany) and *CnGSC* (t1216aep; Broun et al., 1999), were among this downregulated set of head-specific genes (Fig. 7B). Of those, *HyALX*, *CNGSC*, *Wnt7*, *FGF* and *HyTCF* recover their normal expression levels within 3 h making these genes candidates for direct targets of Notch signalling. The organizer gene *CNGSC* was also downregulated and recovered expression after 3 h. However, it was then downregulated again at 6 h. This unusual expression behaviour might indicate the presence of an inhibitory feedback mechanism responding to Notch signalling.

By contrast, the NR genes that were specifically expressed in endodermal foot cells and in ectodermal basal disc cells were largely upregulated in response to Notch inhibition. These include *TGF-4* (t25624aep; Watanabe et al., 2014) and a predicted secreted Wnt inhibitor APCDD1 (t11061aep). Thus, Notch inhibition by DAPT resulted in reciprocal regulation of foot and head genes in *Hydra*, with genes normally expressed at the oral end being downregulated and genes normally expressed at the aboral end being upregulated (Fig. 7B).

These data indicate that Notch signalling regulates gene expression in battery cells and further head patterning genes, including the canonical Wnt signalling components HyWnt7 and HyTCF, whereas the BMP pathway component TGF-4 as well as a secreted Wnt inhibitor, both expressed in the foot, appeared to be negatively regulated by Notch.

Promoter analysis of NR genes reveals likely direct targets of Notch signalling

The differential gene expression analysis revealed sets of genes that showed shared behaviour after Notch inhibition and re-activation after DAPT removal. This suggests shared regulation, and hence we performed a motif enrichment analysis to uncover respective regulatory elements in genes with similar expression dynamics. This analysis was done for the following gene sets: (1) downregulated only at 0 h, (2) downregulated at 0 and 3 h, (3) downregulated at 0, 3 and 6 h, (4) upregulated only at 0 h, (5) upregulated at 0 and 3 h, and (6) upregulated at 0, 3 and 6 h. Regions of open chromatin, as identified by previously published ATAC-seq data, within 5 kb upstream of each gene were considered in the enrichment analysis (see Fig. 8 and Materials and Methods for details) (Siebert et al., 2019).

The group of genes that were downregulated in response to DAPT treatment and then recovered normal expression by 3 h are the best candidates for being direct targets of Notch signalling. If genes are direct targets of Notch signalling, we would expect to find RBPJ-binding sites (Kopan and Ilagan, 2009). In line with our prediction, the RBPJ motif (Bailey and Posakony, 1995) was enriched in NR genes of this group (Table S1; Fig. 8B). Among the 21 genes with RBPJ-binding sites in their regulatory region, *HyAlx* (t16456aep)

Journal of Cell Science (2021) 134, jcs258768. doi:10.1242/jcs.258768

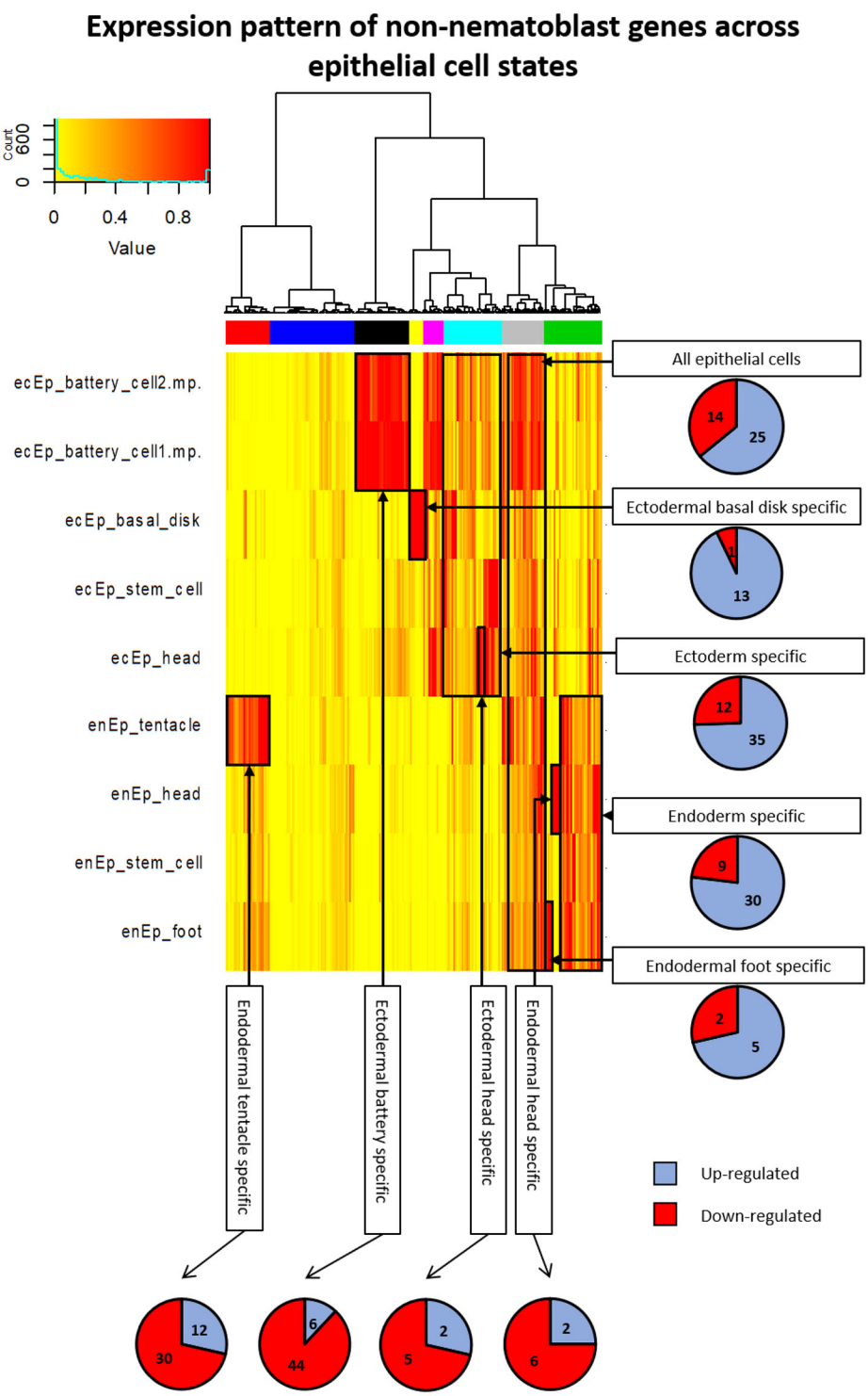

Fig. 6. NR gene subset with expression in epithelial cells. Non-nematoblast NR genes were clustered separately to determine their expression in epithelial cell states. This revealed sets of genes that are most strongly expressed in endodermal tentacle cells (red cluster), ectodermal basal disc cells (yellow), ectodermal battery cells (black), body column ectoderm cells (cyan), body column endoderm cells (green) and all epithelial cells (grey). The analysis also revealed smaller gene sets expressed in endodermal foot cells, endodermal head cells or ectodermal head cells. Tentacle, battery and head-specific genes were mainly downregulated upon DAPT treatment whereas the genes in the remaining clusters were mainly upregulated. The colour key refers to cell state expression values. The green line in the small diagram indicates the distribution of *z*-scores.

and *Sp5* (t29291aep), with six RBPJ motifs, are the top candidates for direct targets of Notch signalling (Fig. 8D,E; Table S1). We also identified the transcription factors pituitary homeobox 1-like (specifically expressed in head cells of the endoderm, t5275aep) and a homeobox protein of the OTX-family (t33622aep). Putative RBPJ motifs were additionally present in genes encoding potential membrane or extracellular proteins, including a foot-specific secreted frizzled-related protein, a potential regulator of Wnt signalling (t15331aep, annotation provided by Bert Hobmayer, Innsbruck, Austria, personal communication).

In addition to the RBPJ-binding site, we found enrichment of further transcription factor-binding motifs belonging to 10 transcription factor families. Homeobox transcription factors were the most abundant motifs identified and several different HMG, forkhead and bHLH motifs were also found (Table S1). Interestingly, this corresponds with the downregulation of transcription factors that potentially bind to these domains, for example, HyHES (bHLH), Jun (bZIP), FoxP1 (Forkhead), HyAlx, (homeobox, t16456aep), OTX-related (homeobox, t33622aep) and PITX-related factors (homeobox, t5275aep) and three SOX-related

Journal of Cell Science (2021) 134, jcs258768. doi:10.1242/jcs.258768

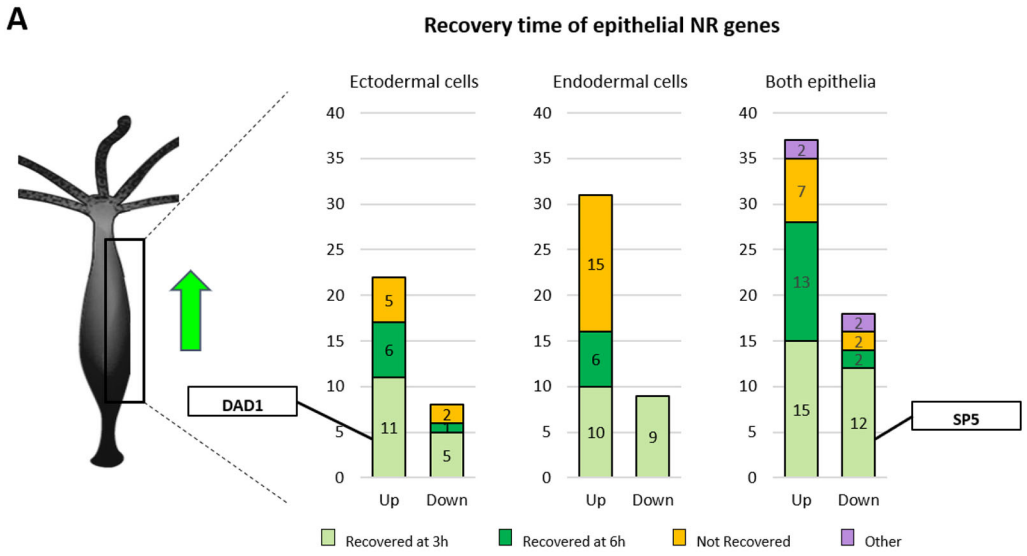

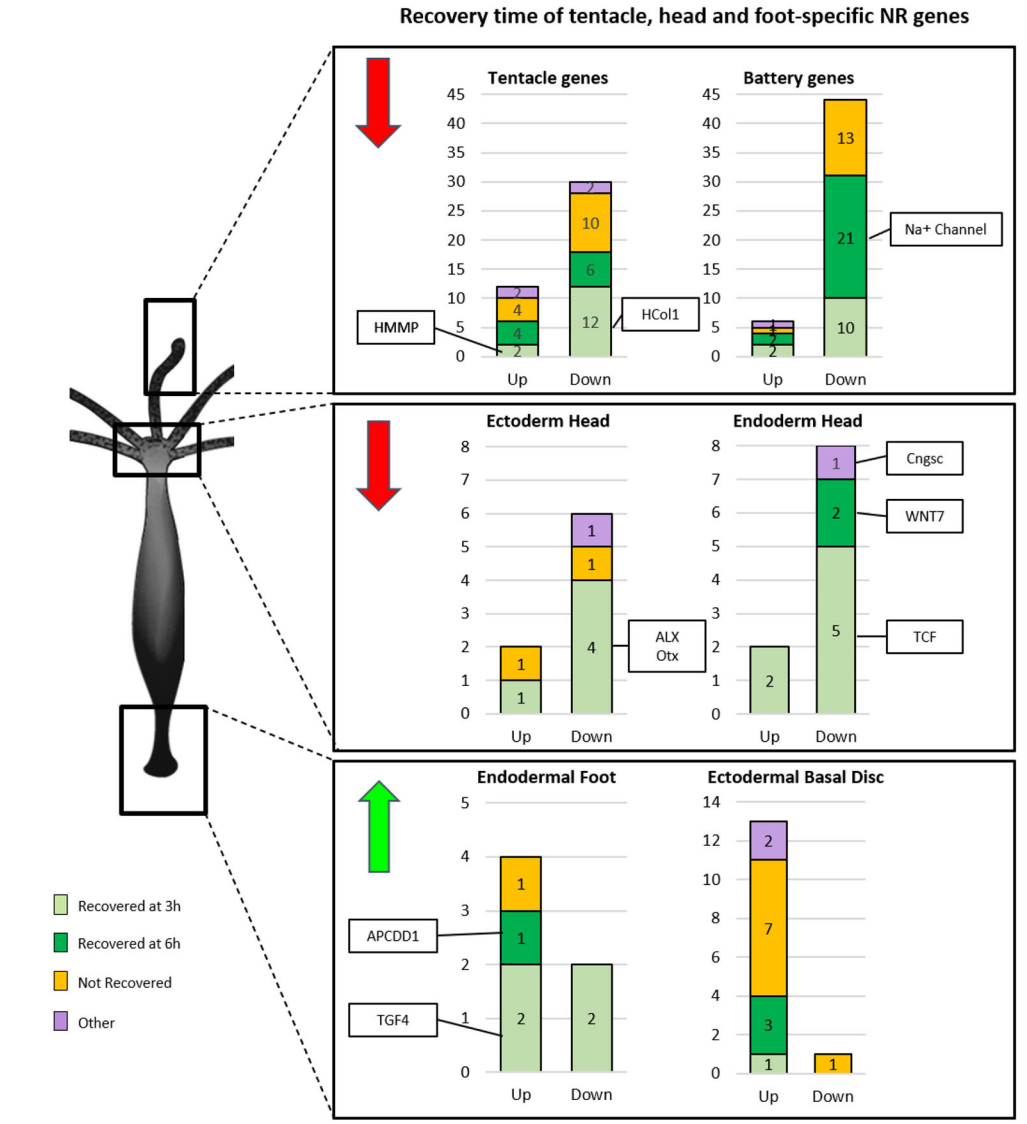

Fig. 7. Recovery time of NR genes. (A) The majority of epithelial NR genes were upregulated upon DAPT treatment. 50% of the upregulated ectodermal-specific NR genes recover expression within the first 3 h post-DAPT removal (light green) and include the apoptosis-involved gene DAD1. SP5 on the other hand, which is expressed in both epithelia, is downregulated and recovers expression also within the first 3 h. (B) Head-specific fNR genes, including tentacle, battery and ectodermal and endodermal head genes, are mostly downregulated upon DAPT treatment. In contrast, foot-specific genes, including endodermal foot genes and basal disc genes are mostly upregulated. Many of these genes play a predominant role in patterning.

Journal of Cell Science (2021) 134, jcs258768. doi:10.1242/jcs.258768

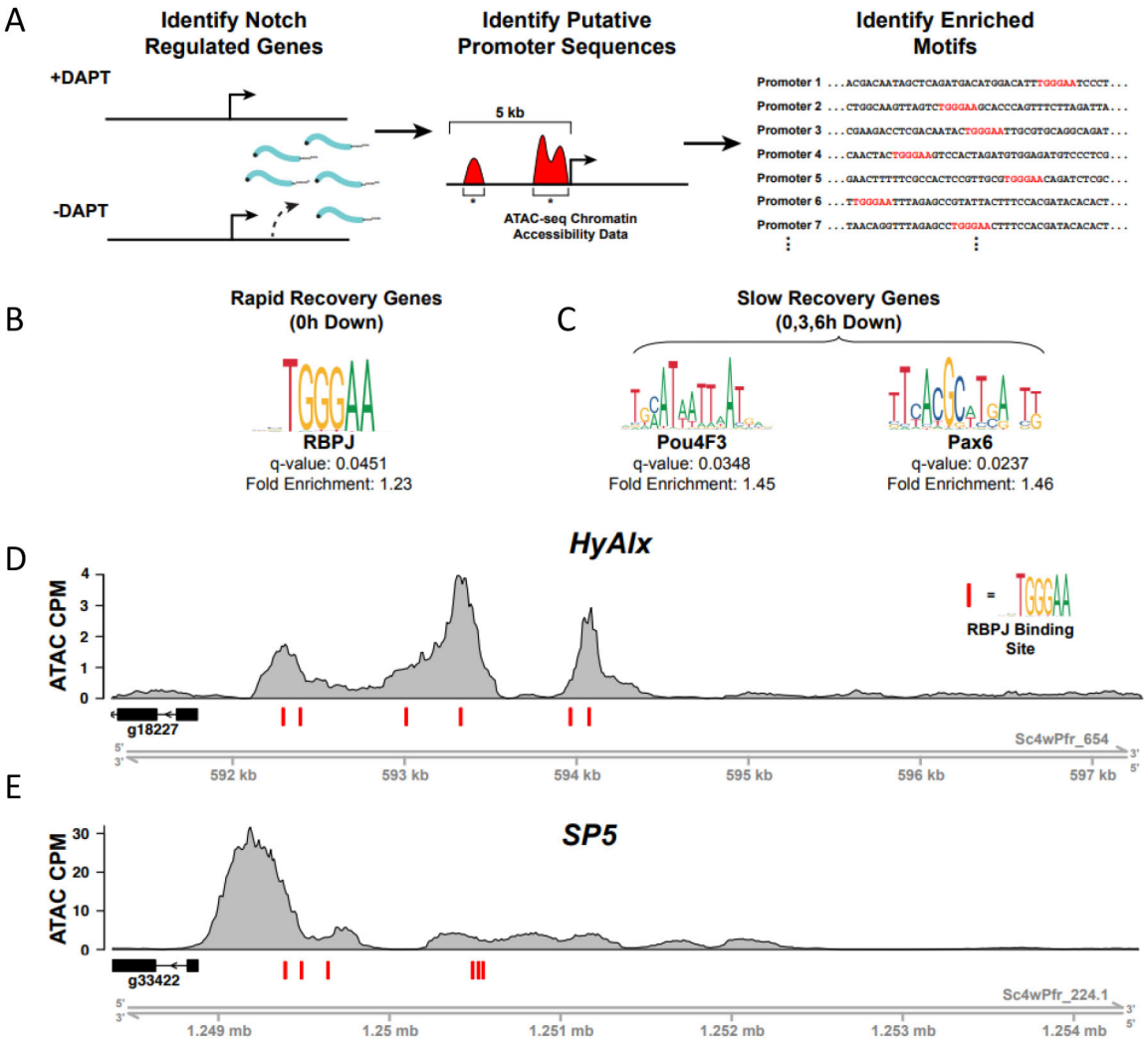

Fig. 8. Motif enrichment analysis of NR gene promoter regions. (A) Workflow of motif enrichment analysis. Putative promoter regions were identified using a previously published ATAC-seq dataset generated using whole wild-type *Hydra* (Siebert et al., 2019). NR gene promoter regions were defined as ATAC-seq peaks that fell within 5 kb upstream of the transcription start site of an NR gene. Using HOMER, NR gene promoters were compared against control peaks that were not associated with NR genes to identify significantly enriched (FDR≤0.05) transcription factor-binding motifs. (B) Notch/RBPJ-binding motifs were significantly enriched in the putative promoters of genes that were downregulated upon DAPT treatment and recovered rapidly following inhibitor removal. (C) Pou and Pax transcription factor binding motifs were significantly enriched in the putative promoters of genes that were downregulated upon DAPT treatment and did not recover their expression over the course of the RNA-seq experiment. Plots of normalized ATAC-seq read density in the 5 kb upstream of (D) HyAlx and (E) SP5 demonstrate the presence of predicted RBPJ-binding sites in the putative promoters of NR genes. Red bars indicate predicted instances of Notch-binding motifs.

proteins (HMG-boxes, t23837aep, t23172aep, t5528aep) [see Tables S1, S2, S3; an alignment and phylogeny is available via FigShare (doi:10.6084/m9.figshare.14714169)]. Therefore, these data reveal the possible components of a gene regulatory network influenced by Notch signalling.

For the group of genes downregulated at all three time points, six enriched motifs were found, most notably POU- and PAX-binding motifs (Fig. 8C; Table S1). The *POU*-gene has previously been implicated in nematocyte differentiation and was found enriched in genes expressed at late stages of nematogenesis (Siebert et al., 2019). *HyPOU4TF-2 like* was downregulated by Notch inhibition at 0 and 3 h (Table S2). The three predicted *Hydra-Pax*-genes [t9974aep, t6559aep and t11467aep, see table (doi:10.6084/m9.figshare.14681343) and alignment and phylogeny (doi:10.6084/m9.figshare.14714169) on FigShare] were not amongst the NR genes.

In the group of genes that were upregulated at 0 h, but recovered by 3 h, only the IRF9-binding motif (interferon regulatory factor) was found enriched. For genes that were upregulated at 0 and 3 h, but recovered expression at 6 h, many bZIP-factor-binding motifs were enriched.

As expected, this analysis uncovered RBPJ-binding sites in several NR genes. Of those, and in accordance with their quick recovery after DAPT removal, HyAlx and HySp5, each with six putative RBPJ-sites appeared to be the strongest candidates for direct transcriptional targets of Notch signalling, followed by a negative regulator of Wnt signalling (secreted frizzled-related protein) and the potential transcriptional repressor MAD, which has a hypothetical function in regulating proliferation in epithelia cells.

DISCUSSION

Inhibiting Notch signalling induces a block in nematocyte differentiation and disrupts head patterning in *Hydra* (Münder et al., 2013). Comparable Notch effects have also been described in

Journal of Cell Science (2021) 134, jcs258768. doi:10.1242/jcs.258768

two other cnidarian model organisms, namely *Nematostella* and *Hydractinia* (Gahan et al., 2017; Layden and Martindale, 2014; Marlow et al., 2012; Richards and Rentzsch, 2015). In this study, we have identified Notch-regulated (NR) genes by analysing RNA-seq data obtained at different timepoints after treatment of *Hydra* polyps with DAPT. Exploration of the *Hydra* single-cell gene expression atlas (Siebert et al., 2019) revealed sets of genes that were expressed in cell states consistent with observed inhibition phenotypes. Moreover, in many NR genes, we detected binding sites for DNA-binding protein RBPJ – the principal effector of Notch signalling.

Unexpectedly, we detected upregulation of genes encoding heat shock proteins and proteins involved in apoptosis (see table 'Functional annotation of NR genes' at doi:10.6084/m9.figshare.14681319), hinting at a stress response of the animals to the treatment, which we can attribute to DAPT, as effects of the solvent DMSO should be hidden in our experimental design. Promoter analysis of those upregulated genes revealed enrichment of a Trp-cluster motif (IRF9, Table S1). This motif is targeted by the interferon regulatory factor as part of a stress and anti-viral defence pathway in mammals (Jefferies, 2019). Its occurrence and function in *Hydra* genes should be elucidated in the future.

Strikingly, almost half of the Notch-responsive genes were expressed in cells of the nematocyte lineage; 99% of those were downregulated and expressed in post-mitotic nematoblast stages. This reflected Notch regulation of a gene module specific to post-mitotic nematoblasts that are in the process of capsule formation. In this module, we find genes that have been previously shown to encode structural capsule proteins, such as minicollagens (Engel et al., 2001), spinalin (Koch et al., 1998), NOWA (Engel et al., 2002), nematogalectin (Zhang et al., 2019), N-col15 (Adamczyk et al., 2008), nematocilin (Hwang et al., 2008) and others. Moreover, we find transcription factors like HyPOU (Siebert et al., 2019) and CnASH (Grens et al., 1995). This is consistent with Notch-inhibition blocking differentiation and the initiation of a transcription programme for capsule formation. We propose that HyPOU is involved in executing this programme, but that it is not a direct Notch target since expression is not re-established within 3 h. In accordance with this hypothesis, motif enrichment analysis identified POU4F DNA-binding motifs in the putative regulatory region of genes that did not recover from DAPT within 6 h. Similarly, *CnASH* expression does not recover within 6 h, confirming it as an indirect or secondary target (Fig. S1). In contrast, the potential *Hydra Jun* gene, which encodes a C-terminal bZIP-Jun-domain protein, did recover expression levels fast (Table S2) whereas bZIP-binding motifs appeared to be enriched in promoters of downregulated genes that remained downregulated for 6 h post treatment (Table S1). Recent work in *Nematostella* had indicated the Jun-homolog *Cnido-Jun* is involved in driving nematogenesis, as knockdown of *Cnido-Jun* resulted in loss of expression of *NvNcol3* (Nv is *Nematostella vectensis*) and defects in nematocyte morphology (Sunagar et al., 2018). The mammalian transcription factor JUN is part of the activator-protein 1 (AP-1) transcription factor complex, which responds to numerous extracellular signals including MAP-kinase and cytokine signalling as a reaction to environmental signals. AP-1 is also known as a driver of differentiation in the immune system (reviewed in Katagiri et al., 2021). It is tempting to speculate that Notch controls AP-1-like transcriptional regulation in *Hydra* (Fig. S4B). This could be a mediator for adjusting nematogenesis in adult animals to nutrient-dependent requirements for nematocyte production from precursors. In starving animals, for instance, mature nematocytes are not used, thus turnover is low and this governs replenishment (Yaross and Bode, 1978).

Genes that are expressed in nematoblast precursors, including *HyZIC* (Lindgens et al., 2004) and the *Hydra Pax-2A* homolog (t9974aep) were not affected by DAPT. This is also true for the *Hydra* homolog of *Myc*, *Hymyc1* (Hartl et al., 2010), the human homolog of which is a Notch target gene in mammals (Giaimo et al., 2021).

Genes that are potentially directly targeted by the NICD would not only be expected to recover their expression level quickly when DAPT treatment is removed and NICD is allowed to enter the nucleus but would be expected to also contain RBDJ sites in their promoter regions. Such binding motifs have been detected in a number of nematocyte-specific genes with unknown function (Table S3). These genes do not encode transcription factors, suggesting that the NICD directly activates the nematocyte differentiation gene complex. Future studies will reveal their role during nematoblast differentiation and also whether they can account for the missing differentiation cue that is directly blocked with DAPT.

However, as an alternative explanation, failure to carry out the nematoblast differentiation programme in our experiments could be caused by missing patterning signals from the *Hydra* head. This hypothesis is suggested because of the strong head phenotypes that we had previously described after DAPT inhibition. The first observable phenotype after 48 h of Notch inhibition was a substantial shortening of the tentacles. Moreover, transplantation experiments with GFP-labelled body column tissue indicated that, during the time of Notch inhibition, cells did not cross the boundary between body column and tentacles (Münder et al., 2013). A 'neck-like' structure appeared underneath the tentacle zone, where cells had ceased proliferating, but also did not differentiate into battery cells. In this study, we reveal a cluster of downregulated head-specific genes among the genes that are dysregulated in response to Notch inhibition.

Of particular interest is the *aristaless*-related gene *HyALX*, which has six potential RBPJ sites in its putative regulatory region. Our study strongly suggests that Notch signalling directly activates *HyALX* expression. *HyALX* has previously been proposed to instruct the specification of tentacle tissue (Smith et al., 2000), and we suggest that *HyAlx* could play this key role in directing tentacle fate by activating genes with homeobox transcription factor-binding motifs. In support of this, we found that the homeobox motif was enriched in the NR genes downregulated by DAPT that recover their expression quickly after DAPT removal (Table S1). Another potential Notch target with five RBPJ sites in its promoter region is the Max-dimerisation domain (MAD)-encoding *MAD* gene. This is part of the MYC/Max/MAD network of transcription factors that are involved in the regulation of cell proliferation. MAD forms heterodimers with the bHLH transcription factor MAX, which often mediates repression of proliferative gene activity (Lüscher, 2012). This could also play a role at the tentacle boundary where proliferation of epithelial cells is stopped when they pass into tentacles and become battery cells.

HyALX is expressed in evenly spaced rings at the body column–tentacle boundaries. After release of DAPT inhibition it rapidly recovers expression levels, yet it does not recover a regular expression pattern but becomes expressed in irregular rings, and in extreme cases is in only one ring surrounding the whole animal (Münder et al., 2013). Assuming that NICD acts as a direct activator of *HyALX*, this indicates that Notch signalling is resumed in the wrong places. Therefore, a feedback mechanism can be suggested,

where the Notch signalling pattern depends on the head organizer, which in turn is co-instructed by Notch signalling.

The potential *Hydra* head organizer gene *CnGSC* (Broun et al., 1999) is downregulated by Notch inhibition and does not recover its activity after 6 h. Furthermore, *Wnt7*, *TCF* and *Sp5*, genes implicated in the canonical Wnt signalling pathway (Broun et al., 1999; Lengfeld et al., 2009; Vogg et al., 2019), are also downregulated. In contrast, we found a small cluster with foot and peduncle genes that were upregulated, including the BMP-pathway gene *TGF-4* (Watanabe et al., 2014). Together, these data may guide the uncovering of molecular pathways responsible for the irregularly shaped heads that develop in polyps after a 48 h period of DAPT treatment (Münder et al., 2013). They also confirm a role of Notch signalling in establishing and maintaining the *Hydra* head organizer, which was previously discovered in transplantation experiments, where the organizer capacity of regenerating *Hydra* head tissue had been inhibited by DAPT (Münder et al., 2013).

The role of Notch signalling for the maintenance of tentacle boundaries can be explained when HyAlx and Sp5 are direct targets for activation by NICD. Expression of HyAlx would then always be maintained by a strong Notch signal at the tentacle boundary. Sp5 would also be expressed in response to this Notch signal to block the activity and expression of canonical Wnts at the boundary. All canonical Wnt genes are expressed in the head outside the tentacle zone. Non-canonical Wnt signalling, on the other hand, does not appear to be affected by NICD and therefore the PCP pathway is active at the boundary and guides movements of cells into tentacles (Fig. S4A).

Conclusion

This study suggests target genes of Notch signalling in *Hydra*, and provides a resource for the investigation of molecular mechanisms by which HvNotch affects patterning, maintenance of the head organizer and post-mitotic nematocyte differentiation. The expression of the only direct HvNotch target gene, for which experimental evidence is available, *HyHes*, was also found among NR genes, which quickly recovered original expression levels after DAPT removal. We have identified *HyAlx* and *Sp5* as prime candidates for further direct HvNotch targets involved in head patterning due to their quick recovery after DAPT relief and the presence of RBPJ sites in their promoter regions. A candidate for a direct HvNotch target gene expressed in differentiating nematoblast states and quickly recovering from DAPT treatment is HyJun. As a component of the AP1 transcription complex, it might synchronise nematocyte differentiation as a response to the demand for mature nematocytes depending on usage. Moreover, the impact of HvNotch on regulation of this differentiation step might be conveyed by inducing expression of genes encoding proteins other than transcription factors, for instance genes that are required to form the post-Golgi vacuole. It has to be considered that many genes with as-yet-unknown functions are amongst potential direct Notch targets in nematoblasts.

MATERIALS AND METHODS

Hydra culture

Animals of the strain *Hydra vulgaris* (Basel) were grown in *Hydra* medium (0.1 mM KCl, 1 mM NaCl, 0.1 mM $MgSO_4$, 1 mM Tris and 1 mM $CaCl_2$) at 18°C and fed regularly with freshly hatched *Artemia nauplii*.

DAPT treatment

Regularly fed animals were starved for 24 h and incubated in either 20 µM DAPT with 1% DMSO in *Hydra* medium or in only 1% DMSO in *Hydra* medium (control sample) for 48 h. DAPT and DMSO were renewed every 12 h. Animals were collected, and total RNA was isolated at three different time points: directly at the end of 48 h (0 h), 3 h after DAPT removal (3 h) and 6 h after DAPT removal (6 h). After 48 h incubation, DAPT was removed and replaced with 1% DMSO in *Hydra* medium for the samples 3 h and 6 h. About 25 animals were collected per sample. Six biological replicates were analysed for RNA-seq respectively, two biological replicates (with three technical replicates each) were used for qPCR (Fig. S1).

qPCR

For each sample, total RNA was extracted from 25 whole animals using the RNeasy Mini kit Plus (Qiagen) according to the manufacturer's protocol at time points of 0 h (48 h of DAPT treatment), 2 h, 5.5 h, 8 h, 10 h and 24 h after DAPT removal, for both DAPT-treated and control (1% DMSO only) animals. RNA quality and quantity were assessed using an Agilent Bioanalyzer. RNA with a RIN value of at least 8 was used for cDNA synthesis using the iScript cDNA synthesis kit (BioRad) according to manufacturer's protocol. A non-RNA and non-reverse transcriptase control were included.

Primers for qPCR were designed using the NCBI primer designing tool (https://www.ncbi.nlm.nih.gov/tools/primer-blast/) (*HyHES*, fw 5′-CCCA-CCACCTAGTCCTTCTTC-3′, rev 5′-TTCTGCTTGGGCAAGTTTGG-3′; *CnASH*, fw 5′-AGACGTTCTAGTCATAGTGTTGTC-3′, rev 5′-AGC-CATCATTGACCTGCTTTAC-3′) and tested to ensure they amplified the correct fragment from cDNA by gel electrophoresis. Gene-specific primer pairs that yielded one melt peak and a linear standard curve were used for qPCR quantification.

cDNA was diluted 1:25 to ensure the used concentration was within the standard curve of the primers. qPCR with SYBR green detection was performed using an CFX96 Touch Real-Time PCR Detection System (BioRad). Each measurement was performed in three technical replicates. A no template control (NTC) was included. The genes *RPL13*, *EF1α* and *PPIB* served as housekeeping genes and their geomean was used for normalization. The samples were analysed on a 96-well plate in a CFX96 Touch Real-Time PCR Detection System from BioRadRelative expression was calculated as 2^-(*dCt*(test sample)−*dCt*(reference sample)). The error bars represent the s.e.m. (Fig. S1).

Immunohistochemistry

Animals were briefly (1–2 min) relaxed in 2% urethane in *Hydra* medium and fixed immediately after in 2% paraformaldehyde in *Hydra* medium for 1 h. Animals were washed with PBS, permeabilized with 0.5% Triton-X-100/PBS (15 min) and blocked with 0.1% Triton-X-100/1% BSA/PBS (20 min). Primary antibodies were applied overnight at 4°C. After a PBS-wash, animals were incubated with secondary antibodies (2 h), washed again with PBS, counterstained for DNA with DAPI (Sigma, 1 µg/ml) and mounted on slides in Vectashield mounting medium (Axxora).

Whole-mount *in situ* hybridization

RNA *in situ* hybridization experiments were carried out as previously described (Grens et al., 1995) using digoxigenin labelled RNA probes (Roche) and substrates NBT/BCIP or BM Purple (Roche).

RNA-seq

RNA-seq libraries were prepared for six biological replicates for each experimental condition. cDNA libraries were synthesized from total RNA using the strand-specific SENSE mRNA-Seq Library Prep Kit V2 for Illumina (Lexogen) and the Purification Module with Magnetic Beads (Lexogen). The samples were multiplexed and sequenced on three lanes on Illumina Hiseq2000 with a 100 bp paired end sequencing strategy. Downstream analyses were performed using the Galaxy platform and within R [RStudio Team (2016); version 1.1.463; RCode provided at doi:10.6084/m9.figshare.14681310]. Illumina adapters and polyA sequences were trimmed and splice leader sequences (Stover and Steele, 2001) were removed from both forward and reverse reads. The tool 'fastqfilter' was used to ensure the paired nature of the filtered dataset, to filter out reads with a quality score lower than 20 and to exclude reads with a read length shorter than 30 bp. Reads that contained 'N's were also removed from the dataset.

De novo transcriptome assembly

All forward and all reverse reads from all sequencing libraries were concatenated. The two resulting files were then used as input to the Trinity (version 2.8.4; Grabherr et al., 2011) *de novo* transcriptome assembler. The assembly was run with the following parameters: -strand-specific library, *in silico* normalisation, -min_contig_length 300, -min_kmer_cov 1, no genome guided mode and no Jaccard Clip options. The resulting reference transcriptome resulted in 62,419 transcripts (43,481 genes) with an average transcript length of 1008b and a median length of 588 bp. A total of 10% of the genes have an average length of 5017 bp and 50% of them are 1495 bp in average. The average GC content of all genes was 34.7%. Transcripts that belonged to the same gene were joined to form SuperTranscripts (tool 'Generate SuperTranscripts from a Trinity assembly'; Galaxy version 2.8.4), which were then used for local Blast search. These were treated as genes models in downstream analyses (see below).

Mapping reads to transcriptome

The processed reads of the 36 RNA-seq libraries (timepoints 0, 3 and 6 h, DAPT and control samples, six replicates) were separately mapped to the *de novo* assembled transcriptome reference, within the Galaxy platform. The reads were mapped as strand-specific and with a maximum insert size of 800. RSEM (Li and Dewey, 2011) – with Bowtie2 (Langmead and Salzberg, 2012; Langmead et al., 2009) as alignment method – was used as the abundance estimation method. The overall alignment rate was >95% for all samples except for one control sample, which had an alignment rate of only 88%. The transcript alignment files of all samples and the gene_to_transcript_map were used as input to generate an expression matrix for all 43,481 assembled genes.

Differential expression analysis

The raw counts were used as input for differential expression (DE) analysis by DESeq2 (version 1.18.1). Genes that were not detected in all 36 samples were excluded from this analysis. DE analysis was performed for each time point separately by comparing the DAPT treatment replicates with those from the control animals (0 h DAPT versus 0 h DMSO, 3 h DAPT versus 3 h DMSO and 6 h DAPT versus 6 h DMSO). Differentially expressed genes at time point 0 h were selected according to their *P*-adjusted value [Padj (FDR) <0.01]. We refer to this gene set as Notch-regulated genes (NR genes). For each of these NR genes, we investigated whether DE was also identified at time points 3 h and 6 h, thereby applying the same cutoff for DE [Padj (FDR) <0.01].

Blast search

Several blast searches were performed to annotate NR genes. The NCBI *Hydra vulgaris* protein database (on 2020.02.24) was interrogated using blastx. Sequences with no blast hit or a blast hit with an E-value $>10\times10^{-100}$ were blasted manually. Three types of manual blast searches were performed, NCBI blastn and blastx and NCBI smartBLAST (full list of NR genes on Figshare; doi:10.6084/m9.figshare.14681343). Sequences for which no blast hits were found in either blast search were denoted with 'no blast hit'. This was also the case for sequences, for which a blast hit was found but with an E-value $>10\times10^{-20}$. For the genes that were blasted manually, the NCBI description and accession number was replaced by those of the blast hit with the highest E-value and query cover (for example, if the manual blastn search yielded a better hit than the local blast to the NCBI protein database). The PubMed accession number was added for known Hydra genes. Uniprot was used to search for information about the function and the compartment of the identified sequences, these were denoted as 'unclear' in cases it was unclear or unknown. Multiple alignments were performed for genes with a similar TrinityID and genes with similar/same NCBI description.

Cell state analysis

To make use of the available Hydra single-cell data, we first identified NR genes within the single-cell transcriptome reference using blastn (Siebert et al., 2019) (Transcriptome Shotgun Assembly project; GHHG01000000; see https://www.ncbi.nlm.nih.gov/geo/query/acc.cgi?acc=GSM4009036). Duplicated hits were removed by keeping the alignments with the highest blast score. Existing Seurat data objects were used to retrieve expression data and cell state annotations (Siebert et al., 2019; and see related data on Dryad at https://doi.org/10.5061/dryad.v5r6077). For hierarchical clustering approaches, average cluster expression was calculated for each cell state (Seurat_2.3.4::AverageExpression). Seurat objectes were then subsetted to the NR gene set and expression was scaled from 0 to 1. Hierarchical clustering was performed using functions stats::dist('euclidian') and stats::hclust('ward.D'). A heatmap (gplots_3.0.0::heatmap.2) with the scaled average expression was generated.

NMF analysis

Normalized expression information was extracted from the whole transcriptome Seurat object for each DE gene with an AEP reference and used for non-negative matrix factorization (NMF) analysis. This analysis was performed as described by Siebert and colleagues (Siebert et al., 2019).

Motif enrichment analysis

To identify putative promoter regions of NR genes, we used a previously published ATAC-seq dataset generated from whole wild-type *Hydra* (Siebert et al., 2019) to locate regions of accessible chromatin (i.e. peaks) within 5 kb upstream of NR gene transcription start sites. We then grouped these NR promoter regions based on the expression dynamics of their putative target genes in our DAPT-treated RNA-seq time course. A total of six sets of NR genes were considered for downstream motif enrichment analyses: (1) genes that were downregulated but recovered by 3 h post-treatment, (2) genes that were downregulated but recovered by 6 h post treatment, (3) genes that were downregulated and remained downregulated at 6 h post treatment, (4) genes that were upregulated but recovered by 3 h post treatment, (5) genes that were upregulated but recovered by 6 h post-treatment, and (6) genes that were upregulated and remained upregulated at 6 h post treatment.

For our motif enrichment analysis, we used a curated set of known transcription factor binding motifs provided by the JASPAR database (Fornes et al., 2020). Specifically, we used position weight matrices from the non-redundant vertebrate, insect, nematode and urochordate JASPAR datasets. JASPAR-formatted position weight matrices were converted to HOMER-formatted motifs using the HOMER parseJasparMatrix function. HOMER-formatted motifs require the specification of a score threshold that is used for identifying true motif hits in a query sequence. No such score threshold is included in JASPAR-formatted motifs, so we manually set the threshold to be 40% of the maximum possible score (i.e. the score that would be received by a sequence that perfectly matches the canonical binding sequence) for each motif.

We then used this custom set of HOMER motifs to identify transcription factor-binding motifs that were significantly enriched in each of the six abovementioned NR peak sets. We did this by comparing the NR peak sets to non-NR peaks using a binomial enrichment test as implemented in the HOMER findMotifsGenome function. Motif enrichment results were then filtered using a false discovery rate threshold of $\leq$0.05.

We found that our raw HOMER results included numerous enriched motifs with highly similar sequences. To simplify these results, we sought to identify and remove redundant motifs from the results tables. To accomplish this, we first generated a matrix of pairwise similarity scores for all motifs in our custom motif set using the HOMER compareMotifs function. These similarity scores were then used to perform hierarchical clustering to identify groups of highly similar motifs. We then reduced the redundancy of our enrichment results by including only the most significantly enriched motif from each motif cluster in the final results table.

To identify putative RBPJ-binding sites in NR promoter regions, we used the HOMER scanMotifGenomeWide function to find sequences that matched the RBPJ and Su(H) binding motifs (JASPAR matrix IDs MA1116.1 and MA0085.1, respectively). In addition, we also made use of a custom Su(H) motif based on a previously reported description of the Su(H) consensus binding site (Bailey and Posakony, 1995). The custom HOMER Su(H) motif was generated using the HOMER seq2profile function; the score threshold was set to be 40% of the maximum possible score.

Plots of ATAC-seq read density and predicted RBPJ-binding sites were generated using the R Gviz package (Hahne and Ivanek, 2016). ATAC-seq reads from individual biological replicates were pooled before generating read density plots.

Acknowledgements
The Galaxy platform of Blum's group at the Gencentre Munich was used for read processing.

Competing interests
The authors declare no competing or financial interests.

Author contributions
Conceptualization: A.B., J.M., C.J., S.S.; Methodology: J.M., S.S., S.K., J.C., A.P.; Software: J.M., S.S., S.K., J.C.; Validation: A.B., J.M., S.S.; Formal analysis: J.M., J.C., A.P., Q.P.; Investigation: A.B., J.M., S.K., J.C., A.P., Q.P.; Resources: J.M.; Data curation: A.B., J.M., J.C., A.P., C.J.; Writing - original draft: A.B., J.M.; Writing - review & editing: J.M., A.B., S.S., C.J.; Visualization: J.M., J.C., A.P., Q.P.; Supervision: A.B.; Project administration: A.B.; Funding acquisition: A.B., C.J.

Funding
This work was funded by Deutsche Forschungsgemeinschaft grant BO1748-12-1 awarded to A.B. and the National Institutes of Health grant R35GM133689 awarded to C.J. Deposited in PMC for release after 12 months.

Data availability
Information available on FigShare comprises the full list of NR genes, doi:10.6084/m9.figshare.14681343; functional annotation of NR genes, doi:10.6084/m9.figshare.14681319; alignment and phylogeny, doi:10.6084/m9.figshare.14714169; Supplementary RCode, doi:10.6084/m9.figshare.14681310; Assembled Trinity SuperTranscripts, doi:10.6084/m9.figshare.14999946.

Peer review history
The peer review history is available online at https://journals.biologists.com/jcs/article-lookup/doi/10.1242/jcs.258768

References
Adamczyk, P., Meier, S., Gross, T., Hobmayer, B., Grzesiek, S., Bachinger, H.P., Holstein, T.W. and Ozbek, S. (2008). Minicollagen-15, a novel minicollagen isolated from Hydra, forms tubule structures in nematocysts. *J. Mol. Biol.* **376**, 1008-1020. doi:10.1016/j.jmb.2007.10.090

Alexandrova, O., Schade, M., Böttger, A. and David, C. N. (2005). Oogenesis in Hydra: nurse cells transfer cytoplasm directly to the growing oocyte. *Dev. Biol.* **281**, 91-101. doi:10.1016/j.ydbio.2005.02.015

Andersson, E. R., Sandberg, R. and Lendahl, U. (2011). Notch signaling: simplicity in design, versatility in function. *Development* **138**, 3593-3612. doi:10.1242/dev.063610

Bailey, A. M. and Posakony, J. W. (1995). Suppressor of hairless directly activates transcription of enhancer of split complex genes in response to Notch receptor activity. *Genes Dev.* **9**, 2609-2622. doi:10.1101/gad.9.21.2609

Borggrefe, T. and Oswald, F. (2009). The Notch signaling pathway: transcriptional regulation at Notch target genes. *Cell. Mol. Life Sci.* **66**, 1631-1646. doi:10.1007/s00018-009-8668-7

Bosch, T. C. G. and David, C. N. (1986). Male and female stem cells and sex reversal in Hydra polyps. *Proc. Natl. Acad. Sci. USA* **83**, 9478-9482. doi:10.1073/pnas.83.24.9478

Broun, M., Sokol, S. and Bode, H. R. (1999). Cngsc, a homologue of goosecoid, participates in the patterning of the head, and is expressed in the organizer region of Hydra. *Development* **126**, 5245-5254. doi:10.1242/dev.126.23.5245

David, C. N. and Campbell, R. D. (1972). Cell cycle kinetics and development of Hydra attenuata. I. Epithelial cells. *J. Cell Sci.* **11**, 557-568. doi:10.1242/jcs.11.2.557

David, C. N. and Gierer, A. (1974). Cell cycle kinetics and development of Hydra attenuata. III. Nerve and nematocyte differentiation. *J. Cell Sci.* **16**, 359-375. doi:10.1242/jcs.16.2.359

Deutzmann, R., Fowler, S., Zhang, X., Boone, K., Dexter, S., Boot-Handford, R. P., Rachel, R. and Sarras, M. P.Jr (2000). Molecular, biochemical and functional analysis of a novel and developmentally important fibrillar collagen (Hcol-I) in hydra. *Development* **127**, 4669-4680. doi:10.1242/dev.127.21.4669

Engel, U., Pertz, O., Fauser, C., Engel, J., David, C. N. and Holstein, T. W. (2001). A switch in disulfide linkage during minicollagen assembly in Hydra nematocysts. *EMBO J.* **20**, 3063-3073. doi:10.1093/emboj/20.12.3063

Engel, U., Ozbek, S., Streitwolf-Engel, R., Petri, B., Lottspeich, F. and Holstein, T. W. (2002). Nowa, a novel protein with minicollagen Cys-rich domains, is involved in nematocyst formation in Hydra. *J. Cell Sci.* **115**, 3923-3934. doi:10.1242/jcs.00084

Fang, T. C., Yashiro-Ohtani, Y., Del Bianco, C., Knoblock, D. M., Blacklow, S. C. and Pear, W. S. (2007). Notch directly regulates Gata3 expression during T helper 2 cell differentiation. *Immunity* **27**, 100-110. doi:10.1016/j.immuni.2007.04.018

Fedders, H., Augustin, R. and Bosch, T. C. (2004). A Dickkopf- 3-related gene is expressed in differentiating nematocytes in the basal metazoan Hydra. *Dev. Genes Evol.* **214**, 72-80. doi:10.1007/s00427-003-0378-9

Fornes, O., Castro-Mondragon, J. A., Khan, A., van der Lee, R., Zhang, X., Richmond, P. A., Modi, B. P., Correard, S., Gheorghe, M., Baranasic, D. et al. (2020). JASPAR 2020: update of the open-access database of transcription factor binding profiles. *Nucleic Acids Res.* **48**, e87-e92. doi:10.1093/nar/gkaa516

Gahan, J. M., Schnitzler, C. E., DuBuc, T. Q., Doonan, L. B., Kanska, J., Gornik, S. G., Barreira, S., Thompson, K., Schiffer, P., Baxevanis, A. D. et al. (2017). Functional studies on the role of Notch signaling in Hydractinia development. *Dev. Biol.* **428**, 224-231. doi:10.1016/j.ydbio.2017.06.006

Gauchat, D., Escriva, H., Miljkovic-Licina, M., Chera, S., Langlois, M. C., Begue, A., Laudet, V. and Galliot, B. (2004). The orphan COUP-TF nuclear receptors are markers for neurogenesis from cnidarians to vertebrates. *Dev. Biol.* **275**, 104-123. doi:10.1016/j.ydbio.2004.07.037

Geling, A., Steiner, H., Willem, M., Bally-Cuif, L. and Haass, C. (2002). A gamma-secretase inhibitor blocks Notch signaling in vivo and causes a severe neurogenic phenotype in zebrafish. *EMBO Rep.* **3**, 688-694. doi:10.1093/embo-reports/kvf124

Giaimo, B. D., Gagliani, E. K., Kovall, R. A. and Borggrefe, T. (2021). Transcription factor RBPJ as a molecular switch in regulating the notch response. *Adv. Exp. Med. Biol.* **1287**, 9-30. doi:10.1007/978-3-030-55031-8_2

Golubovic, A., Kuhn, A., Williamson, M., Kalbacher, H., Holstein, T. W., Grimmelikhuijzen, C. J. and Gründer, S. (2007). A peptide-gated ion channel from the freshwater polyp Hydra. *J. Biol. Chem.* **282**, 35098-35103. doi:10.1074/jbc.M706849200

Grabherr, M. G., Haas, B. J., Yassour, M., Levin, J. Z., Thompson, D. A., Amit, I., Adiconis, X., Fan, L., Raychowdhury, R., Zeng, Q. et al. (2011). Full-length transcriptome assembly from RNA-Seq data without a reference genome. *Nat. Biotechnol.* **29**, 644-652. doi:10.1038/nbt.1883

Grens, A., Mason, E., Marsh, J. L. and Bode, H. R. (1995). Evolutionary conservation of a cell fate specification gene: the Hydra achaete-scute homolog has proneural activity in Drosophila. *Development* **121**, 4027-4035. doi:10.1242/dev.121.12.4027

Hahne, F. and Ivanek, R. (2016). Visualizing genomic data using gviz and bioconductor. *Methods Mol. Biol.* **1418**, 335-351. doi:10.1007/978-1-4939-3578-9_16

Hartl, M., Mitterstiller, A.-M., Valovka, T., Breuker, K., Hobmayer, B. and Bister, K. (2010). Stem cell-specific activation of an ancestral myc protooncogene with conserved basic functions in the early metazoan Hydra. *Proc. Natl. Acad. Sci. USA* **107**, 4051-4056. doi:10.1073/pnas.0911060107

Hobmayer, B., Rentzsch, F., Kuhn, K., Happel, C. M., von Laue, C. C., Snyder, P., Rothbächer, U. and Holstein, T. W. (2000). WNT signalling molecules act in axis formation in the diploblastic metazoan Hydra. *Nature* **407**, 186-189. doi:10.1038/35025063

Holstein, T. W., Hobmayer, E. and David, C. N. (1991). Pattern of epithelial cell cycling in hydra. *Dev. Biol.* **148**, 602-611. doi:10.1016/0012-1606(91)90277-A

Hwang, J. S., Takaku, Y., Chapman, J., Ikeo, K., David, C. N. and Gojobori, T. (2008). Cilium evolution: identification of a novel protein, nematocilin, in the mechanosensory cilium of Hydra nematocytes. *Mol. Biol. Evol.* **25**, 2009-2017. doi:10.1093/molbev/msn154

Jarrett, S. M., Seegar, T. C. M., Andrews, M., Adelmant, G., Marto, J. A., Aster, J. C. and Blacklow, S. C. (2019). Extension of the Notch intracellular domain ankyrin repeat stack by NRARP promotes feedback inhibition of Notch signaling. *Sci. Signal.* **12**, eaay2369. doi:10.1126/scisignal.aay2369

Jefferies, C. A. (2019). Regulating IRFs in IFN driven disease. *Front. Immunol.* **10**, 325. doi:10.3389/fimmu.2019.00325

Käsbauer, T., Towb, P., Alexandrova, O., David, C. N., Dall'armi, E., Staudigl, A., Stiening, B. and Böttger, A. (2007). The Notch signaling pathway in the cnidarian Hydra. *Dev. Biol.* **303**, 376-390. doi:10.1016/j.ydbio.2006.11.022

Katagiri, T., Kameda, H., Nakano, H. and Yamazaki, S. (2021). Regulation of T cell differentiation by the AP-1 transcription factor JunB. *Immunol. Med.* doi:10.1080/25785826.2021.1872838.

Koch, A. W., Holstein, T. W., Mala, C., Kurz, E., Engel, J. and David, C. N. (1998). Spinalin, a new glycine- and histidine-rich protein in spines of Hydra nematocysts. *J. Cell Sci.* **111**, 1545-1554. doi:10.1242/jcs.111.11.1545

Kopan, R. and Ilagan, M. X. (2009). The canonical Notch signaling pathway: unfolding the activation mechanism. *Cell* **137**, 216-233. doi:10.1016/j.cell.2009.03.045

Krejci, A., Bernard, F., Housden, B. E., Collins, S. and Bray, S. J. (2009). Direct response to Notch activation: signaling crosstalk and incoherent logic. *Sci. Signal.* **2**, ra1. doi:10.1126/scisignal.2000140

Langmead, B. and Salzberg, S. L. (2012). Fast gapped-read alignment with Bowtie 2. *Nat. Methods* **9**, 357-359. doi:10.1038/nmeth.1923

Langmead, B., Trapnell, C., Pop, M. and Salzberg, S. L. (2009). Ultrafast and memory-efficient alignment of short DNA sequences to the human genome. *Genome Biol.* **10**, R25. doi:10.1186/gb-2009-10-3-r25

Lasi, M., Pauly, B., Schmidt, N., Cikala, M., Stiening, B., Käsbauer, T., Zenner, G., Popp, T., Wagner, A., Knapp, R. T. et al. (2010). The molecular cell death machinery in the simple cnidarian Hydra includes an expanded caspase family and pro- and anti-apoptotic Bcl-2 proteins. *Cell Res.* **20**, 812-825. doi:10.1038/cr.2010.66

Layden, M. J. and Martindale, M. Q. (2014). Non-canonical Notch signaling represents an ancestral mechanism to regulate neural differentiation. *Evodevo* **5**, 30. doi:10.1186/2041-9139-5-30

Lengfeld, T., Watanabe, H., Simakov, O., Lindgens, D., Gee, L., Law, L., Schmidt, H. A., Ozbek, S., Bode, H. and Holstein, T. W. (2009). Multiple Wnts are involved in Hydra organizer formation and regeneration. *Dev. Biol.* **330**, 186-199. doi:10.1016/j.ydbio.2009.02.004

Leontovich, A. A., Zhang, J., Shimokawa, K., Nagase, H. and Sarras, M. P.Jr (2000). A novel hydra matrix metalloproteinase (HMMP) functions in extracellular matrix degradation, morphogenesis and the maintenance of differentiated cells in the foot process. *Development* **127**, 907-920. doi:10.1242/dev.127.4.907

Liao, B.-K. and Oates, A. C. (2017). Delta-Notch signalling in segmentation. *Arthropod. Struct. Dev.* **46**, 429-447. doi:10.1016/j.asd.2016.11.007

Lindgens, D., Holstein, T. W. and Technau, U. (2004). Hyzic, the Hydra homolog of the zic/odd-paired gene, is involved in the early specification of the sensory nematocytes. *Development* **131**, 191-201. doi:10.1242/dev.00903

Lüscher, B. (2012). MAD1 and its life as a MYC antagonist: an update. *Eur. J. Cell Biol.* **91**, 506-514. doi:10.1016/j.ejcb.2011.07.005

Marlow, H., Roettinger, E., Boekhout, M. and Martindale, M. Q. (2012). Functional roles of Notch signaling in the cnidarian Nematostella vectensis. *Dev. Biol.* **362**, 295-308. doi:10.1016/j.ydbio.2011.11.012

Micchelli, C. A., Esler, W. P., Kimberly, W. T., Jack, C., Berezovska, O., Kornilova, A., Hyman, B. T., Perrimon, N. and Wolfe, M. S. (2003). Gamma-secretase/presenilin inhibitors for Alzheimer's disease phenocopy Notch mutations in Drosophila. *FASEB J.* **17**, 79-81. doi:10.1096/fj.02-0394fje

Mumm, J. S. and Kopan, R. (2000). Notch signaling: from the outside in. *Dev. Biol.* **228**, 151-165. doi:10.1006/dbio.2000.9960

Münder, S., Käsbauer, T., Prexl, A., Aufschnaiter, R., Zhang, X., Towb, P. and Böttger, A. (2010). Notch signalling defines critical boundary during budding in Hydra. *Dev. Biol.* **344**, 331-345. doi:10.1016/j.ydbio.2010.05.517

Münder, S., Tischer, S., Grundhuber, M., Buchels, N., Bruckmeier, N., Eckert, S., Seefeldt, C. A., Prexl, A., Käsbauer, T. and Böttger, A. (2013). Notch-signalling is required for head regeneration and tentacle patterning in Hydra. *Dev. Biol.* **383**, 146-157. doi:10.1016/j.ydbio.2013.08.022

Otto, J. J. and Campbell, R. D. (1977). Tissue economics of hydra: regulation of cell cycle, animal size and development by controlled feeding rates. *J. Cell Sci.* **28**, 117-132. doi:10.1242/jcs.28.1.117

Prexl, A., Münder, S., Loy, B., Kremmer, E., Tischer, S. and Böttger, A. (2011). The putative Notch ligand HyJagged is a transmembrane protein present in all cell types of adult Hydra and upregulated at the boundary between bud and parent. *BMC Cell Biol.* **12**, 38. doi:10.1186/1471-2121-12-38

Richards, G. S. and Rentzsch, F. (2015). Regulation of Nematostella neural progenitors by SoxB, Notch and bHLH genes. *Development* **142**, 3332-3342. doi:10.1242/dev.123745

Roboti, P. and High, S. (2012). The oligosaccharyltransferase subunits OST48, DAD1 and KCP2 function as ubiquitous and selective modulators of mammalian N-glycosylation. *J. Cell. Sci.* **125**, 3474-3484. doi:10.1242/jcs.103952

Siebel, C. and Lendahl, U. (2017). Notch signaling in development, tissue homeostasis, and disease. *Physiol. Rev.* **97**, 1235-1294. doi:10.1152/physrev.00005.2017

Siebert, S., Farrell, J. A., Cazet, J. F., Abeykoon, Y., Primack, A. S., Schnitzler, C. E. and Juliano, C. E. (2019). Stem cell differentiation trajectories in Hydra resolved at single-cell resolution. *Science* **365**, eaav9314. doi:10.1126/science.aav9314

Smith, K. M., Gee, L. and Bode, H. R. (2000). HyAlx, an aristaless-related gene, is involved in tentacle formation in hydra. *Development* **127**, 4743-4752. doi:10.1242/dev.127.22.4743

Steele, R. E. (2002). Developmental signaling in Hydra: what does it take to build a "simple" animal? *Dev. Biol.* **248**, 199-219. doi:10.1006/dbio.2002.0744

Stover, N. A. and Steele, R. E. (2001). Trans-spliced leader addition to mRNAs in a cnidarian. *Proc. Natl. Acad. Sci. USA* **98**, 5693-5698. doi:10.1073/pnas.101049998

Sudhop, S., Coulier, F., Bieller, A., Vogt, A., Hotz, T. and Hassel, M. (2004). Signalling by the FGFR-like tyrosine kinase, Kringelchen, is essential for bud detachment in Hydra vulgaris. *Development* **131**, 4001-4011. doi:10.1242/dev.01267

Sunagar, K., Columbus-Shenkar, Y. Y., Fridrich, A., Gutkovich, N., Aharoni, R. and Moran, Y. (2018). Cell type-specific expression profiling unravels the development and evolution of stinging cells in sea anemone. *BMC Biol.* **16**, 108. doi:10.1186/s12915-018-0578-4

Vogg, M. C., Beccari, L., Iglesias Olle, L., Rampon, C., Vriz, S., Perruchoud, C., Wenger, Y. and Galliot, B. (2019). An evolutionarily-conserved Wnt3/β-catenin/Sp5 feedback loop restricts head organizer activity in Hydra. *Nat. Commun.* **10**, 312. doi:10.1038/s41467-018-08242-2

Wang, H., Zang, C., Liu, X. S. and Aster, J. C. (2015). The role of Notch receptors in transcriptional regulation. *J. Cell. Physiol.* **230**, 982-988. doi:10.1002/jcp.24872

Watanabe, H., Schmidt, H. A., Kuhn, A., Höger, S. K., Kocagöz, Y., Laumann-Lipp, N., Özbek, S. and Holstein, T. W. (2014). Nodal signalling determines biradial asymmetry in Hydra. *Nature* **515**, 112-115. doi:10.1038/nature13666

Yaross, M. S. and Bode, H. R. (1978). Regulation of interstitial cell differentiation in Hydra attenuata. V. Inability of regenerating head to support nematocyte differentiation. *J. Cell Sci.* **34**, 39-52. doi:10.1242/jcs.34.1.39

Zhang, R., Jin, L., Zhang, N., Petridis, A. K., Eckert, T., Scheiner-Bobis, G., Bergmann, M., Scheidig, A., Schauer, R., Yan, M. et al. (2019). The sialic acid-dependent nematocyst discharge process in relation to its physical-chemical properties is a role model for nanomedical diagnostic and therapeutic tools. *Mar. Drugs* **17**, 469. doi:10.3390/md17080469